

# Paleoceanography and Paleoclimatology

## RESEARCH ARTICLE

10.1029/2020PA004004

### Key Points:

- A high-resolution  $\delta^{13}\text{C}_{\text{carb}}$  record from Cau (Spain) is proposed as a new global reference for stratigraphic correlation of the Aptian
- The ultrahigh-resolution record of the onset of OAE 1a documents a long-term negative excursion in C-isotope values, punctuated by several marked negative spikes
- Evidence for the importance of OM burial as a feedback mechanism in response to increased carbon inputs into the ocean-atmosphere system

### Supporting Information:

- Supporting Information S1

### Correspondence to:

J. M. Castro,  
[jmcastro@ujaen.es](mailto:jmcastro@ujaen.es)

### Citation:

Castro, J. M., Ruiz-Ortiz, P. A., de Gea, G. A., Aguado, R., Jarvis, I., Weissert, H., et al. (2021). High-resolution C-isotope, TOC and biostratigraphic records of OAE 1a (Aptian) from an expanded hemipelagic cored succession, western Tethys: A new stratigraphic reference for global correlation and paleoenvironmental reconstruction. *Paleoceanography and Paleoclimatology*, 36, e2020PA004004. <https://doi.org/10.1029/2020PA004004>

Received 8 JUN 2020

Accepted 29 JAN 2021

## High-Resolution C-Isotope, TOC and Biostratigraphic Records of OAE 1a (Aptian) From an Expanded Hemipelagic Cored Succession, Western Tethys: A New Stratigraphic Reference for Global Correlation and Paleoenvironmental Reconstruction

José M. Castro<sup>1</sup> , Pedro A. Ruiz-Ortiz<sup>1</sup> , Ginés A. de Gea<sup>1</sup> , Roque Aguado<sup>1</sup> , Ian Jarvis<sup>2</sup> , Helmut Weissert<sup>3</sup> , José M. Molina<sup>1</sup> , Luis M. Nieto<sup>1</sup> , Richard D. Pancost<sup>4</sup> , María L. Quijano<sup>1</sup> , Matías Reolid<sup>1</sup> , Peter W. Skelton<sup>5</sup> , Carmina López-Rodríguez<sup>6</sup>, and Rafael Martínez-Rodríguez<sup>1</sup> 

<sup>1</sup>CEACTEMA and Department of Geology, University of Jaén, Campus Universitario, Jaén, Spain, <sup>2</sup>Department of Geography, Geology and the Environment, Kingston University London, Kingston upon Thames, UK, <sup>3</sup>Department of Earth Sciences, ETH Zürich, Zürich, Switzerland, <sup>4</sup>Organic Geochemistry Unit, School of Earth Sciences, School of Chemistry and Cabot Institute for the Environment, University of Bristol, Bristol, UK, <sup>5</sup>Independent Researcher, Milton Keynes, UK, <sup>6</sup>Centro Oceanográfico de Málaga, Spanish Institute of Oceanography (IEO), Fuengirola, Spain

**Abstract** A high-resolution carbonate C-isotope stratigraphy for the Aptian is presented for the Cau core (Spain). The biostratigraphically calibrated C-isotope stratigraphy of the core is used to refine the previously defined C-isotope segments of the Aptian. Thirteen C-isotope segments have been identified and correlated, and further subdivisions are presented. Correlation with other sections worldwide demonstrates the robustness of the C-isotope stratigraphy of the Cau core. The studied succession includes a continuous record of the early Aptian Oceanic Anoxic Event (OAE 1a). Its onset has been studied at an ultrahigh-resolution scale (0.2–0.5 kyr spacing), revealing a succession of sharp  $\delta^{13}\text{C}_{\text{carb}}$  negative spikes, interpreted as a record of pulses of volcanism and methane emissions. The largest spike was rapid (<10 kyr) and marks the base of OAE 1a, which occurs within a longer-term falling  $\delta^{13}\text{C}_{\text{carb}}$  trend. The C-isotope profile across OAE 1a perfectly records the negative (C3/Ap3), positive (C4/Ap4), steady (C5/Ap5), and positive (C6/Ap6) segments that were defined from Cismon (Italy) and subsequently identified worldwide. The Ap7 to Ap14 segments record a C-isotope negative excursion, coupled with high TOC contents, probably related to regional paleogeography. The links with global environmental changes, episodes of widespread deposition of organic matter, and ultimately to major volcanic episodes are discussed. We propose the Cau core as a new reference section for the Aptian, and specifically for OAE 1a, based on its expanded and well-preserved sedimentary, geochemical and biotic archives, which provide further insights into the environmental and biotic changes that occurred during this time interval.

## 1. Introduction

The Aptian (121.4–113.2 Ma, Gradstein et al., 2020) was characterized by a variable greenhouse climate, and was affected by profound perturbations in the carbon cycle, resulting in global changes in climate and environmental conditions, both in marine and continental realms (e.g., Hay, 2017; Skelton, 2003). Some of the most remarkable environmental changes recorded in Aptian sedimentary successions occurred during Oceanic Anoxic Event 1a (OAE 1a; Arthur et al., 1990), which saw widespread elevated burial rates of organic matter in oxygen-depleted ocean bottom waters and/or within expanded oxygen-minimum zones (e.g., the Selli Level of Coccioni et al. (1987)), a nannoconid crisis (Erba, 1994; Erba et al., 2004), the growth and regional demise of carbonate platforms (Castro et al., 2008; Föllmi, 2012; Föllmi et al., 1994; Graziano, 2013; Huck et al., 2010, 2012; Immenhauser et al., 2005; Masse & Fenerci-Masse, 2011; Ruiz-Ortiz et al., 1998; Skelton & Gili., 2012; Skelton et al., 2019; Vahrenkamp, 2010; Weissert et al., 1998; Wissler et al., 2003), and rapid warming followed by cooling events, with possible ice age interludes during the late Aptian (e.g., Bottini & Erba, 2018; Bottini et al., 2015; Davies et al., 2020; Dumitrescu et al., 2006; Erba, 1994; Hochuli et al., 1999; Jenkyns, 2010, 2018; Maurer et al., 2013; McAnena et al., 2013; Naafs & Pancost, 2016;

Weissert & Lini, 1991; Weissert et al., 1998). A rapid rise of atmospheric CO<sub>2</sub> has been invoked as a trigger for OAE 1a, which has been linked to submarine volcanic activity and possibly to methane emissions (Adloff et al., 2020; Bottini et al., 2012, 2015; Erba et al., 2010, 2015; Kuhnt et al., 2011; Leckie et al., 2002; Méhay et al., 2009; Naafs et al., 2016; Weissert & Erba, 2004). In addition to a direct volcanic source of CO<sub>2</sub>, Polteau et al. (2016) have proposed that injection of magma into organic-rich sediments in the High Arctic Large Igneous Province (HALIP) may have forced a massive emission of methane.

The main feedback mechanisms suggested as a response to increases in atmospheric CO<sub>2</sub> are: global warming; short-term shallowing of the calcite compensation depth (CCD), linked to a change in the locus of carbonate deposition from deep to shallow water; accelerated silicate weathering on the continents driving increased carbonate sedimentation rates; higher marine productivity; and the massive burial of organic-rich sediments (Archer, 2010; Berner, 2004; Erba et al., 2015; Jenkyns, 2010, 2018; Skelton & Gili, 2012). Hydrothermal activity associated with LIP submarine volcanism has also been suggested as a driver for increased primary productivity due to iron fertilization, which is especially relevant for productivity by cyanobacteria (e.g., Leckie et al., 2002). Productivity was likely enhanced by a combination of factors including silicate weathering and hydrothermal activity. These processes are considered to have been the main drivers for global perturbations in the C-isotope record during the Aptian.

Major shifts in the C-isotope curve, calibrated with biostratigraphy, provide a robust basis for global correlation, and have been used to subdivide the curve into segments (Menegatti et al., 1998). In this context, a unique magnetic reversal (magnetochron M0) located at the base of the Aptian (Channell et al., 1995), which can be tied to the carbon-isotope stratigraphy, has been proposed to define the base of the Aptian stage (Erba, 1996; Erba et al., 2015; Gradstein et al., 2020). Other stratigraphic markers originally used in Aptian hemipelagic and pelagic successions are beds with high TOC concentrations, but these are not necessarily isochronous, as the episodes of deposition that generate organic-rich levels are often affected by local conditions (Jenkyns, 2010). Nevertheless, the analysis of the stratigraphic distribution of organic-rich levels provides insight into the interplay between local and global conditions during OAEs, including marine productivity and ocean circulation patterns (e.g., Aguado et al., 2014a; Jenkyns, 2010; Quijano et al., 2012).

The main tool for regional to global correlation in Aptian marine sediments is biostratigraphy, which attains its highest resolution by the integration of multiple open-marine fossil groups, mostly of calcareous composition (ammonites, planktonic foraminifera, and calcareous nannofossils; e.g., Aguado et al., 1999, 2014a, 2014b; Bottini & Mutterlose, 2012; Bralower et al., 1995; Coccioni, 2020; Coccioni et al., 1992; Erba et al., 1999; Kennedy et al., 2000; Mutterlose & Böckel, 1998; Najarro et al., 2011). However, the biotic record might also be affected by diachronism of some lowest and highest occurrence datum levels (LO, HO) of key biostratigraphic marker species (Herrle et al., 2004). In addition, certain calcareous fossils may be absent due to the low carbonate content of the sediments that characterize several stratigraphic intervals of the Aptian stage, mostly associated with OAEs, where calcification crises were associated with poor preservation of carbonate (Aguado et al., 2014a, 2014b; Erba, 1994; Erba et al., 2010).

Stable carbon-isotope geochemistry in carbonates and organic matter (OM) has proven to be a useful tool for stratigraphy and environmental history, following the pioneering work of Loutit and Kennett (1979) and Scholle and Arthur (1980), and many others. Integration of chemostratigraphy with biostratigraphy and magnetostratigraphy can improve stratigraphic resolution considerably (Bottini et al., 2015; Bralower et al., 1995; Channell et al., 1995; Dumitrescu et al., 2006; Erba et al., 2015; Tarduno et al., 1989, 1992; Weissert, 2019; Weissert et al., 2008). The C-isotope curve of the Aptian has been calibrated with biostratigraphy and magnetostratigraphy, and it has been divided into several segments which have been widely used for correlation (e.g., Bottini et al., 2015; Bralower et al., 1999; Dumitrescu et al., 2006; Erba et al., 1999, 2015; Herrle et al., 2004; Lorenzen et al., 2013; Menegatti et al., 1998; Sánchez-Hernández & Maurrasse, 2016; Wissler et al., 2002, 2003, 2004; among many others).

Several caveats have to be considered when utilizing geochemical signals as correlation markers (e.g., Scott, 2016). The most important issue is unravelling the effects of diagenesis from the original depositional signal (Weissert et al., 2008), which may lead to significant differences between sections. The consistent definition of divisions (segments) or events and the precision of the curve, a product of sample density with respect to sedimentation rates (Scott, 2016) are crucial, and collectively will control the robustness of any

correlation. Furthermore, the calibration of C-isotope stratigraphy to biostratigraphy, magnetostratigraphy, and absolute ages is necessary to provide numerical estimates that can be used for correlation and testing fundamental questions in the Earth sciences (Gradstein et al., 2020; Malinverno et al., 2012; Martinez et al., 2020; Ogg et al., 2016; Olierook et al., 2019). Here, we use the C3/Ap3 to C6/Ap6 C-isotope segments of Menegatti et al. (1998) for definition of OAE1a. This is the chemostratigraphic interval that corresponds to OAE 1a or the Selli Level equivalent at Cismon (e.g., Bottini et al., 2015; Erba et al., 1999, 2015; Malinverno et al., 2010; Menegatti et al., 1998).

An issue that remains elusive is the pattern of environmental change defining the beginning of OAE 1a. Was the onset of the negative C-isotope excursion C3 (*sensu* Menegatti et al., 1998) rapid, as suggested by analyses of C-isotope patterns in pelagic sediments? Or, was the change in global carbon cycling more gradual—as indicated by a previous study of the hemipelagic western Tethys succession at Cau, southern Spain (Naafs et al., 2016), an outer-shelf expanded sequence deposited on a rifted basin with high subsidence rates, containing most of the Aptian (Castro et al., 2008)?

For this study, we returned to the Cau site, where a core was drilled in 2015–2016 with the aim to establish an improved high-resolution C-isotope curve for the Aptian (Ruiz-Ortiz et al., 2016). One focus of our study was a detailed investigation of the pattern of change in the C-isotope curve at the base of OAE 1a. The nearby field section has been intensively studied and there is a robust database available, including biostratigraphic information for ammonites, planktonic foraminifera, and calcareous nannofossils (Aguado et al., 1999; Castro et al., 2001; de Gea et al., 2003; Moreno-Bedmar et al., 2012), along with a carbonate and organic carbon-isotope ( $\delta^{13}\text{C}_{\text{carb}}$ ,  $\delta^{13}\text{C}_{\text{org}}$ ) stratigraphy (de Gea et al., 2003; Moreno-Bedmar et al., 2012; Naafs et al., 2016), biomarkers (Quijano et al., 2012), and Os isotopes (Adloff et al., 2020). Additionally, a  $p\text{CO}_2$  reconstruction has been developed based on biomarker specific C-isotope values (Naafs et al., 2016) and from that, a carbon-cycle model for the onset of OAE 1a was derived recently by Adloff et al. (2020).

This study, with a focus on the Cau core, presents a high-resolution carbonate C-isotope curve calibrated directly to planktonic foraminifera and calcareous nannofossils, and indirectly to ammonite data from the corresponding field section. This paper provides a new reference C-isotope curve for the Aptian, with a refinement of the previously defined C-isotope segments (Bralower et al., 1999; Herrle et al., 2004; Menegatti et al., 1998) based on high-resolution (~20-cm intervals) sampling (ultrahigh 1-cm resolution, <0.5 kyr sample spacing in some parts of the succession) and calibration to biostratigraphic data. A correlation to other chronostratigraphically well-characterized successions with a precise C-isotope stratigraphy is presented. This highlights the robustness of the C-isotope stratigraphy of the Cau section as a reference for global correlation, and is the basis for discussion on the dynamics of the carbon cycle, environmental and biotic perturbations that occurred during the Aptian. A further advantage of the Cau section is the proximity of neighboring carbonate platform successions, the intimate stratigraphical relations of which with OAE 1a have also been investigated (Skelton et al., 2019).

## 2. Location and Geological Background

The Cau outcrop (38.70389°N, 0.00472°W; 493-m altitude above sea level, D4 borehole, Figure 1) is located in the NE of Alicante Province, southeastern Spain, to the west of Benissa town (Figure 1a). The studied materials represent a continuous record of the Almadich Fm in the area. This lithostratigraphic unit has diachronous lower and upper boundaries, with a maximum stratigraphic range of upper Barremian to uppermost Aptian (Castro et al., 2008); the lower to upper Aptian interval is represented in the Cau outcrops. There, the Almadich Fm lies on a discontinuity surface with a hiatus embracing the Barremian–Aptian transition, developed on the upper Barremian hemipelagic marls and marlstones of the Los Villares Fm (Castro, 1998; Castro et al., 2008), and it is overlain by the shallow platform carbonates of the Seguilí Fm of latest Aptian-earliest Albian age (Castro, 1998; Castro et al., 2008), which represent a progradational episode of the Prebetic platform.

### 2.1. Paleogeographic and Geodynamic Setting

The Cau succession was deposited on the southern margin of the Iberian Plate, on the so-called Southern Iberian Continental Margin (SICM; Martín-Chivelet et al., 2002, 2019; Vera, 2004). At a global scale, the

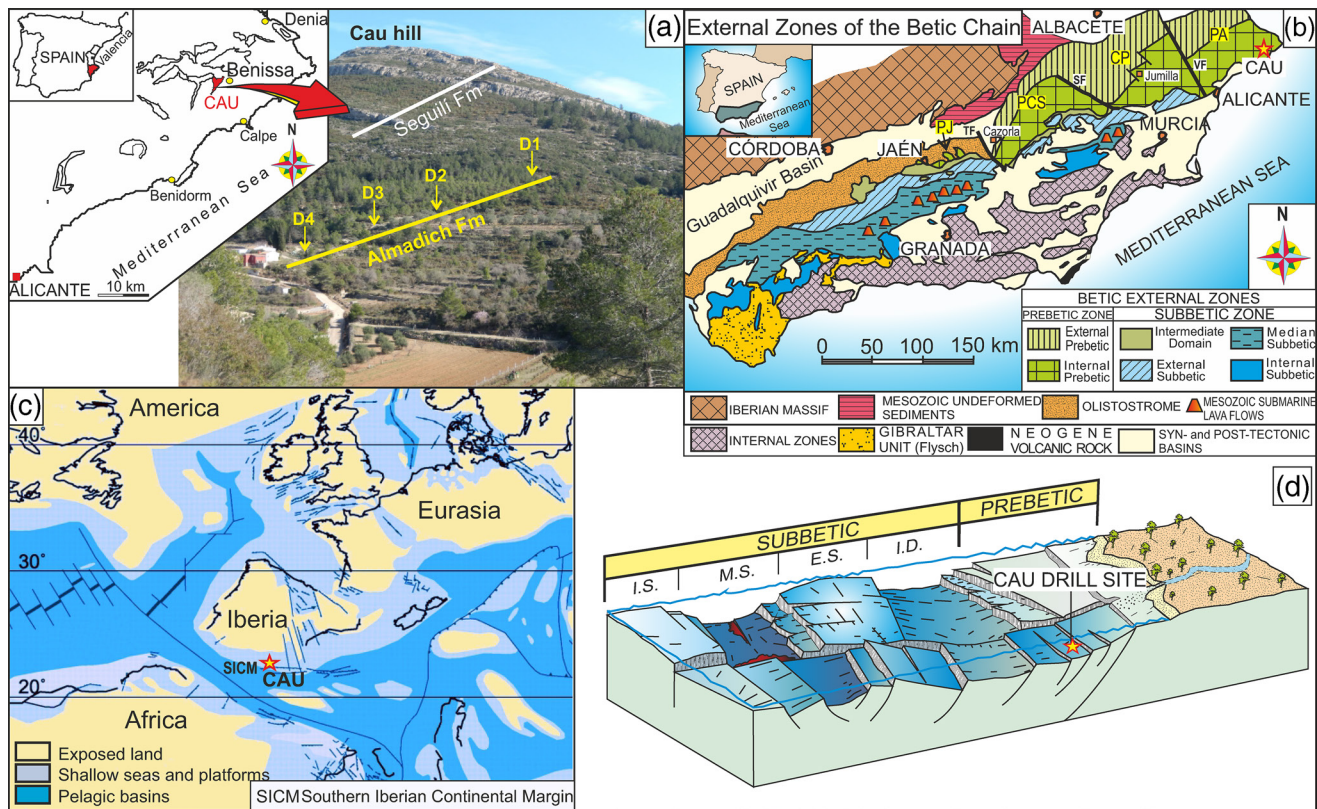


**Figure 1.** (a) Geographic location of the four boreholes (D1–D4) drilled in the Almadich Fm in the Cau hillside located at a horizontal distance (D1–D4) of ca. 100 m. (b) Geological map of the southernmost part of the Iberian Peninsula with the Betic Cordillera, Guadalquivir Basin and southern part of the Iberian Massif; the position of Cau is shown toward the northeastern limit of the map. PJ, Prebetic of Jaén; PCS, Prebetic of Cazorla-Segura; CP, Central Prebetic; PA, Prebetic of Alicante. (c) Early Aptian (~120 Ma) paleogeographic reconstruction of western Tethys (simplified from Masse et al. (2000)) showing the location of Cau on the Southern Iberian Continental Margin (SICM). (d) Reconstruction of the SICM during the Aptian. IS, Internal Subbetic; MS, Median Subbetic; ES, External Subbetic; ID, Intermediate Domain.

SICM was located at the western edge of the western Tethys, along the “seaway” between the Tethys and the Central Atlantic (Figure 1c), and at the antipodes of the major volcanic provinces developed during the Aptian, the Ontong-Java, and Kerguelen plateaus that were intensely active during the early and late Aptian, respectively (e.g., Bralower et al., 1997; Jones & Jenkyns, 2001; Erba et al., 2015). The geodynamic evolution of Iberia during the Aptian was controlled by the relative motions of the Eurasian and African plates. Rotation of Iberia caused by the opening of the Bay of Biscay (Olivet, 1996; Vergès & García-Senz, 2001) led to widespread extension and subsequent rifting in the margins (Figure 1c). Subsidence rates were generally high in the SICM, with thick shallow-water limestone successions (Urgonian facies) deposited on wide carbonate platforms in the proximal parts of the margin, and hemipelagic and pelagic sedimentation in the distal sectors (e.g., Martín-Chivelet et al., 2019, 2002; Vera, 2004).

The Lower Cretaceous stratigraphic succession of the SICM consists of thick units of carbonates and siliciclastics, deposited in two major paleogeographic domains: the shallow Prebetic platform and the pelagic Subbetic basin (Figures 1b and 1d). Both areas were affected by listric faulting, leading to strong lateral differences in subsidence rates (e.g., Martín-Chivelet et al., 2019, 2002; Ruiz-Ortiz, 1980; Vera, 2004) (Figure 1d). The main extensional faults mark the boundaries between tectonic domains, while minor faults generated small subbasins bounded by low-subsidence highs. The tectonic tilting associated with the listric fault geometries favored gradual lateral changes in subsidence rates within the blocks. The stratigraphic succession at Cau corresponds to a depocentre area in the outer part of the Prebetic platform (Figure 1d).

Eustatic and climate changes affected the Aptian sedimentary evolution of the SICM (e.g., Immenhauser, 2005; Immenhauser et al., 1999; Martín-Chivelet et al., 2019). The studied section was located at a paleolatitude of 20–25°N (Masse et al., 1993; Figure 1c), interpreted to lie within the northern part of the

equatorial arid belt (Chumakov et al., 1995). The early Aptian sedimentary evolution of the SICM was impacted by OAE 1a; shallow platforms were subject to an extensive drowning event (e.g., Castro et al., 2014, 2008; Skelton et al., 2019), whereas in outer platform and pelagic settings OAE 1a was marked by the deposition of organic-rich sediments (e.g., Aguado et al., 2014a; de Gea de et al., 2003, 2008).

### 3. Material and Methods

#### 3.1. Fieldwork and Core Processing

Four boreholes were drilled on the western slope of Cau hill, obtained via conventional rotary drilling (Rolatec RL 48 L) using a diamond core drilling system. The four cores had a total recovery of: (D1) 57 m drilled/48 m corrected for dip; (D2) 35/30 m; (D3) 59.5/54 m, and (D4) 39.5/32.5 m. After description and sampling the cores were stored in the Department of Geology at the University of Jaén.

#### 3.2. Carbonate Content

An automatic calcimeter manufactured by DREAM Électronique SAS (Pessac, France), housed in the laboratories of the CEACTierra (University of Jaén), was used to determine the carbonate content of samples.

#### 3.3. Total Organic Carbon (TOC)

TOC analyses were performed in the IRNAS laboratories (CSIC, Sevilla), using a Shimadzu TOC-V CSH instrument.

#### 3.4. C and O Stable Isotopes

Stable isotope ratios from 755 carbonate samples were measured with a ThermoScientific MAT253 Isotope Ratio Mass Spectrometer connected to a Kiel IV Carbonate Device at the Stable Isotope Laboratory of the Instituto de Geociencias, Universidad Complutense de Madrid.

#### 3.5. Sample Processing for Biostratigraphic Analyses

One hundred and twenty-nine samples were prepared on smear slides for calcareous nannofossils investigation, and 54 samples were processed for the determination of planktonic foraminifera assemblages, in the laboratories of the Department of Geology of the University of Jaén.

Description of methods applied is available in the supporting information.

## 4. Results

### 4.1. Facies Analysis

The dominant microfacies throughout the cores is mudstone/wackestone (Dunham, 1962), with varying amounts of fine sand-size grains, dominated by peloids, and variable contents of bioclasts. Other grains present at some levels are fine quartz (up to 15–20%), and rare glauconite and coal particles. Some Fe-oxides and Fe-sulphides are present as grains or diffused in the matrix. The texture is generally homogenous, with a variable degree of bioturbation, although some finely laminated horizons are present. Detailed description has allowed the differentiation of five main facies types (Figure 2): (I) Dark grey massive facies, locally with faint lamination and scarce bioturbation; this facies is common in the OAE 1a interval, and in the upper Aptian, in the *Globigerinelloides algerianus* biozone. (II) Light grey bioturbated facies, with *Chondrites*, *Planolites*, and other feeding, resting, and undefined traces; the intensity of bioturbation is highly variable; Facies II is dominant in the upper Aptian (*Herbergella trocoidea* and *Paraticinella rohri* biozones), and is intercalated with other facies types in the lower part of the core. (III) Dark grey undisturbed mudstones with planar lamination, which are present as thin interbeds within Facies I mostly in the lower Aptian sediments of the OAE 1a interval. (IV) Light to dark grey brecciated to nodular facies with chaotic organization and massive mudstone/wackestone texture irregularly interbedded with partially recrystallized limestone,

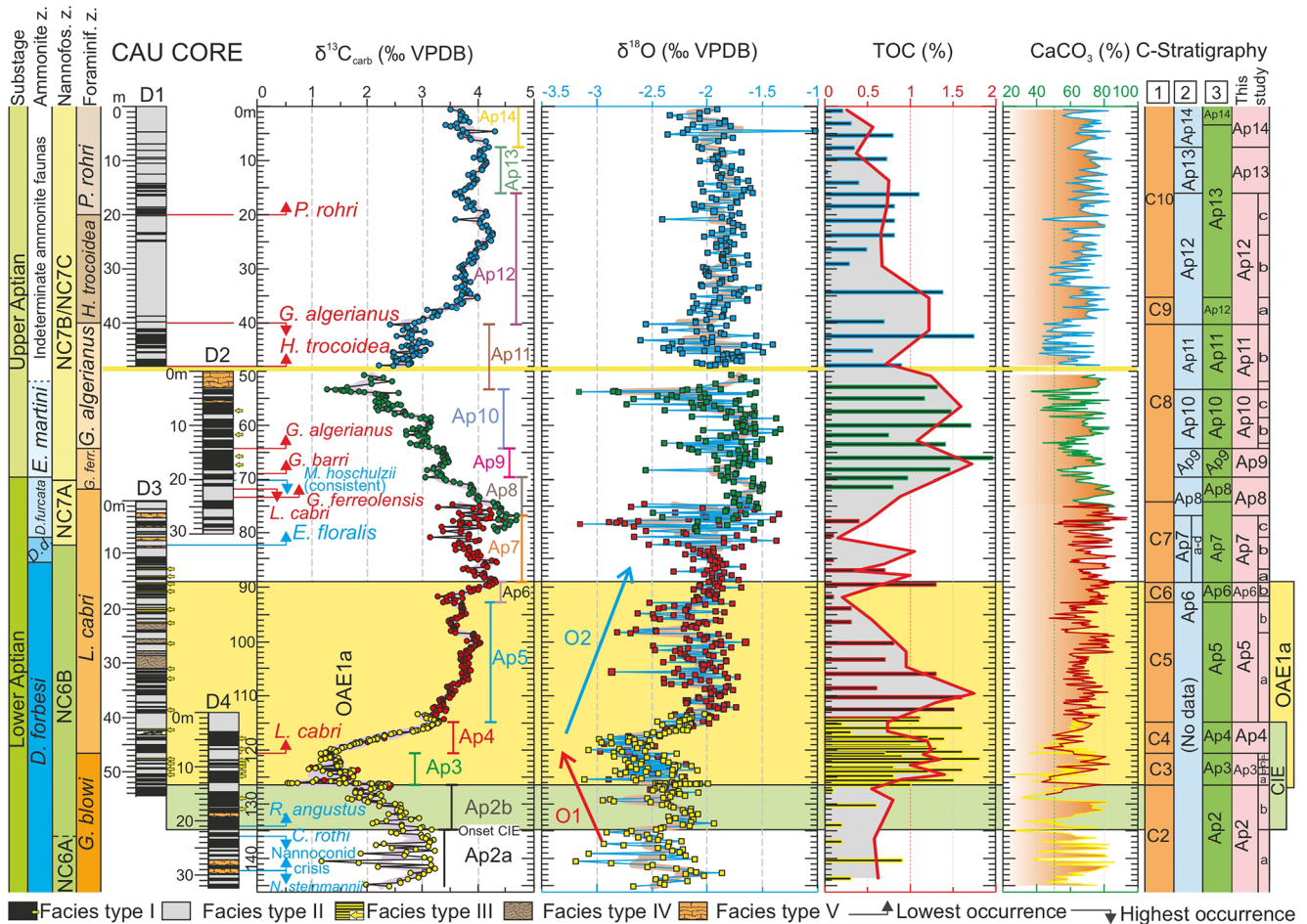


**Figure 2.** Stratigraphy of the Cau core. Biostratigraphy based on nannofossils and foraminifera (core) and ammonites (outcrop). The  $\delta^{13}\text{C}_{\text{carb}}$ ,  $\delta^{18}\text{O}$ , TOC, and  $\text{CaCO}_3$  profiles are represented along with the C-isotope stratigraphy proposed by different authors: (1) Menegatti et al. (1998) and Bralower et al. (1999); (2) Herrle et al. (2004); (3) Bottini et al. (2015), and this study.

present as meter-scale beds in the upper part of the OAE 1a interval (*Leopoldina cabri* biozone). (V) Grey to orange, weathered, recrystallized, or altered facies. This facies type corresponds to the shallowest levels of cores (especially D2 and D3), and single beds in the lowermost part of core D4, and is attributed largely to surficial weathering by interaction with meteoric water.

#### 4.2. Carbonate and TOC

Carbonate contents range generally from 40% to 80%, with a lowest value of 22% and a maximum of 96% (both recorded within D4, *Globigerinelloides blowi* biozone, Figure 2). The vertical trend shows a clear cyclic distribution, with cycle thicknesses of meter scale, and generally gradual transitions between higher to lower carbonate content levels. TOC contents reach a maximum of 2 wt%, with higher contents coinciding with the dark gray levels (facies types I and III). Regression analysis yields a low correlation between TOC and  $\text{CaCO}_3$  ( $R^2 = \text{ca. } 0.06$ ;  $p\text{-value} < 0.00001$ ), which shows that OM contents are almost unaffected by carbonate contents.

#### 4.3. C-Isotope and O-Isotope Stratigraphy

The carbon-isotope values obtained are typical for Aptian hemipelagic and pelagic marlstones and lime-stones (cf. Herrle, 2004; Lorenzen et al., 2013; Menegatti et al., 1998), with  $\delta^{13}\text{C}_{\text{carb}}$  values ranging from 0.67‰ to 4.66‰. An unsmoothed  $\delta^{13}\text{C}_{\text{carb}}$  curve is presented in Figure 2 with identification of the eight

chemostratigraphic segments (C1–C8) defined by Menegatti et al. (1998) and subsequent segments C9 and C10 of Bralower et al. (1999). We also identify the subdivisions proposed by Herrle et al. (2004)—column 2, Figure 2, and by Bottini et al. (2015)—column 3, Figure 2. Furthermore, based on the high-resolution of the profile, we propose here (see Section 5) new subdivisions within the segments previously published, in order to more precisely describe the detailed shifts observed (Ap2–Ap14 and internal subdivisions, Figure 2).

The segments defined by Menegatti et al. (1988) and Bralower et al. (1999) can be identified as follows (Figure 2): the basal part of the succession corresponds to the C2 segment (18.95-m thick), with values increasing in the lower part (Ap2a subsegment) from 2.0‰ to 3.1‰, followed by a general decreasing trend to 2.26‰ punctuated by several negative spikes (Ap2b subsegment). This segment is characterized by marked high-frequency oscillations of higher amplitude (maxima of 2‰) in the lower part, decreasing upwards (average 0.5‰). The base of segment C3 is characterized by a sharp negative shift (from 2.3‰ to 0.49‰), through a 17-cm thick interval. This negative spike has been sampled at a 2-cm spacing, which has revealed a rapid but continuous transition of the C-isotope values. The C3 segment (5.63-m thick) is characterized by a succession of four peaks with a slightly rising trend upwards (from 0.5‰ to 1.1‰), defining cycles with decreasing-upwards amplitudes (Ap3 a to d in Figure 2). The lowest values are attained in the lower part of the segment, drawing an overall negative double-trough shape (see supporting information).

Segment Ap4 represents a gradual change in C-isotope values from 1.09‰ to 3.21‰ through 5.75 m of section. Cyclic fluctuations with an amplitude of <0.2‰ are observed within C4. The Ap5 segment covers a thick interval (21.24-m thick), with relatively stable values ranging from 3.1‰ to 4.03‰ (average of 3.63‰), starting with lower values at the base, and a shift to lower values in its uppermost part (Ap5b). Segment Ap6 marks the end of the stable values, with a minimum value of 3.3‰ at the base (Ap6a) followed by a general positive shift from 3.8‰ to 4.3‰ (Ap6b). The thickness of C6 is 4.12 m. The Ap7 segment (15-m thick) starts with two steps of decreasing C-isotope values (Ap7a and b) followed by an increase of values; 4.3‰ is measured at the base of the segment and 4.0‰ at the top, with a maximum near the top of 4.7‰ (Ap7c). Segments Ap8–Ap10 describe a stepwise falling trend from 4.0‰ to 1.3‰. The Ap11 and Ap12 segments record a gradual positive shift to 4.3‰. Segment Ap13 records slightly decreasing values with 4‰ on average, and segment Ap14 records a positive shift from 4.2‰ to 3.5‰ up to the top of the core.

Oxygen isotope ( $\delta^{18}\text{O}$ ) values vary between  $-3.2\text{‰}$  and  $-1.3\text{‰}$  (Figure 2). They display a long-term evolution with a negative trend (O1) through segments C2–C3 (from ca.  $-2\text{‰}$  to ca.  $-3\text{‰}$ ), followed by a positive tendency (O2) through segments C4–C6 (from ca.  $-3\text{‰}$  to ca.  $-1.8\text{‰}$ ). The upper part (segments C7–C10) shows a generally stable pattern with average values of  $-2.0\text{‰}$ , although with some fluctuations within C7–C8, and greater stability within C9–C10 (Figure 2). The correlation between carbon ( $\delta^{13}\text{C}_{\text{carb}}$ ) and oxygen ( $\delta^{18}\text{O}$ ) isotopes has been evaluated for each core, and for the complete section (Figure 3). In all cases, the regression analysis yields no significant correlation between the two constituents ( $R^2$  ranges between 0.019 and 0.262; Figure 3).

#### 4.4. Biostratigraphy

Nannofossil abundance and diversity in the samples studied were generally inversely related to carbonate content. Samples with low–medium carbonate contents (40–60 wt%) usually contained the best preserved and abundant assemblages. These samples were preferred whenever possible for biostratigraphic determinations. Calcareous nannofossil associations allowed the identification of biozones NC6 (lower Aptian), NC7A (lower–upper Aptian transition), and NC7B–C (upper Aptian) (Figure 2 and Table SI). The main bioevents recorded throughout the Cau core were: (a) the presence of *Hayesites irregularis* and *Nannoconus truitii* from the base of the core; (b) the onset of the nannoconid crisis, coinciding with the highest occurrence (HO) of *Nannoconus steinmannii*, followed by the lowest occurrence (LO) of *Rhagodiscus angustus*, all located within segment Ap2; (c) the LO of *Eprolithus floralis* (Ap7 segment), followed by the end of the consistent record of *Micrantholithus hoschulzii*, located in the uppermost part of segment Ap8. The HO of *Conusphaera rothii*, used as boundary marker to subdivide the NC6 biozone (Bralower et al., 1995), was recorded slightly above the LO of *R. angustus*, from the uppermost part of the Ap2 segment. However, this datum level is not very confident due to the extreme rarity of *C. rothii* in the assemblages from the Cau core and in many other records (e.g., Herrle & Mutterlose, 2003; Moullade et al., 2015).

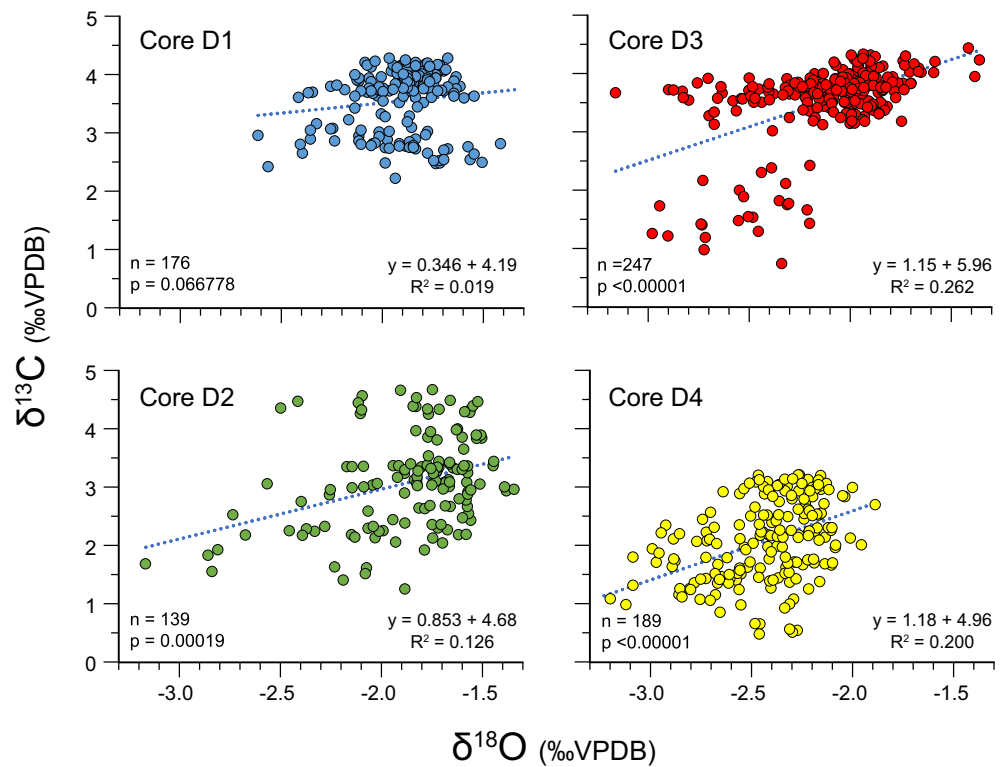


**Figure 3.** Carbonate  $\delta^{13}\text{C}$  vs.  $\delta^{18}\text{O}$  cross-plots for the four cores, D1–D4. A nonsignificant correlation is obtained in all the cases.

The preservation of planktonic foraminifera varies from good to poor, depending on lithology (good in facies I and III). The tests of the specimens were modified by recrystallization, although the original shell texture can be identified in most cases. The mean abundance in productive samples varies from scarce to abundant. Abundance increases in the upper part of core D4 and in the lower and middle parts of core D3, coinciding with OAE 1a. Diversity increases generally upwards, with minor fluctuations linked to changes in abundance. The semiquantitative study has led to the identification of seven genera (*Globigerinelloides*, *Gorbachikella*, *Hedbergella*, *Leupoldina*, *Lilliputianella*, *Paraticinella*, and *Pseudoschackoia*) and 50 species (most of them hedbergellids).

Planktonic foraminifera records (Figure 2) demonstrated the presence of the biozones of *Globigerinelloides blowi* and *Leupoldina cabri* (lower Aptian), *Globigerinelloides ferreolensis*, *Globigerinelloides algerianus*, *Hedbergella trocoidea*, and *P. rohri* (upper Aptian). From bottom to top the following bioevents (Figure 2 and Table SI) were recorded: (a) small-sized trochospiral hedbergellids dominated the assemblages throughout the lower part of the core D4, coinciding with segment Ap2; (b) an increase of hedbergellids with radially elongated chambers (*Hedbergella bizonae*, *H. globulifera*, *H. kuhryi*, and *H. roblesae*) was recorded within segments Ap3–Ap4; (c) the LO of *L. cabri* coincides with the boundary between the Ap3 and Ap4; (d) within segment Ap8, the LO of *G. ferreolensis* is followed by the HO of *L. cabri*; (e) the successive LOs of *Globigerinelloides barri* (lowermost part of Ap9 segment) and *G. algerianus* (Ap9/Ap10 boundary) are recorded; (f) the LO of *H. trocoidea*, located within segment Ap11, is followed by the HO of *G. algerianus* close to the boundary between segments Ap 11 and Ap12; (g) the last bioevent recorded in the core is the LO of *P. rohri* within the upper part of segment Ap12.

Data from the outcrop section (Aguado et al., 1999; Moreno-Bedmar et al., 2012) calibrated to the core (Ap2 to lower part of Ap8 segments) record the presence of the following ammonite biozones: *Deshayesites forbesi*, *Deshayesites deshayesi*, *Dufrenoya furcata*, and *Epicheloniceras martini* (Figure 2). A detailed record of biostratigraphic data calibrated with C-isotope stratigraphy is presented in Table SI.

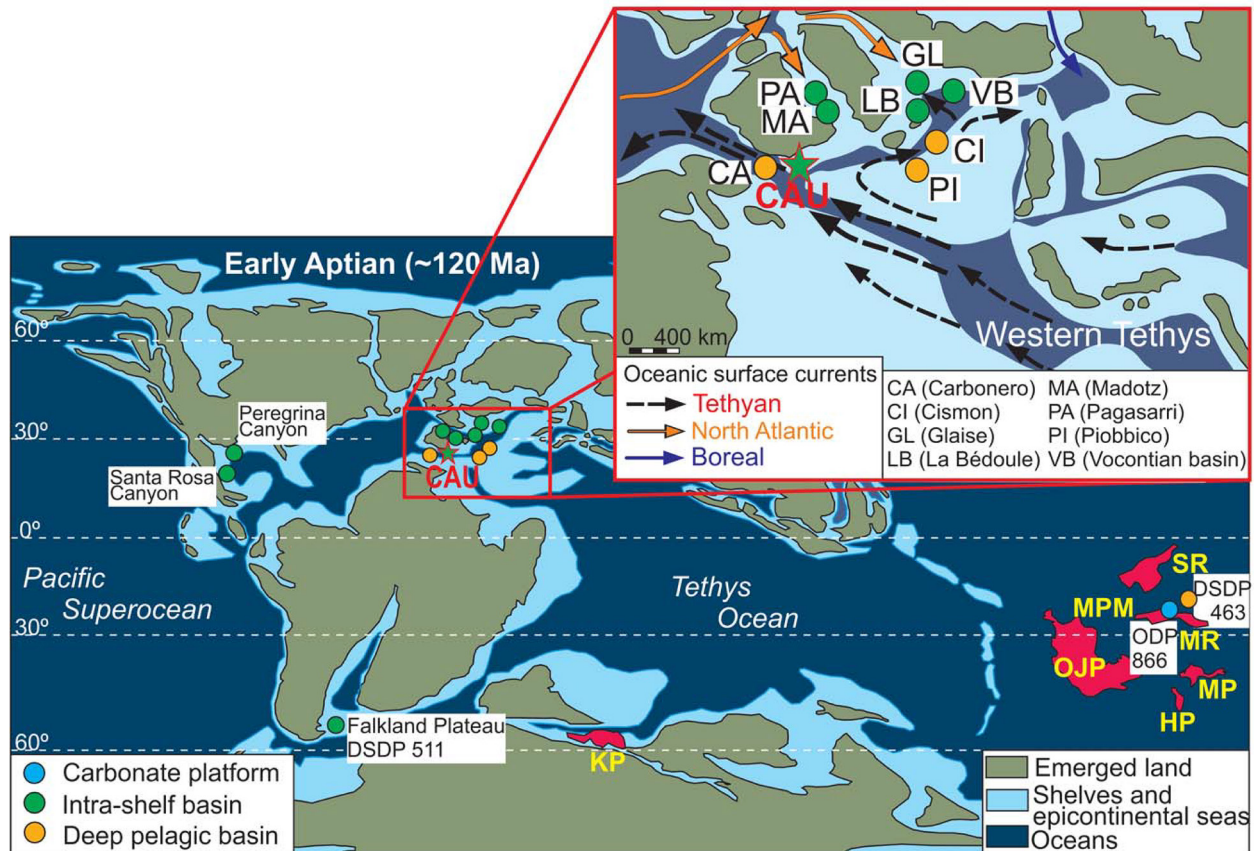


**Figure 4.** Global paleogeography of the Early Cretaceous (~120 Ma), and detailed paleogeographic map of the western Tethys-North Atlantic seaway (modified after Aguado et al. (2018), Blakey (2005), and Dercourt et al. (2000)). Oceanic surface currents are taken from Melinte and Mutterlose (2001) and Misumi and Yamanaka (2008). Key oceanic plateaus are indicated: HP, Hikurangi Plateau; KP, Kerguelen Plateau; MP, Manihiki Plateau; MPM, Mid-Pacific Mountains; MR, Magellan Rise; OJP, Ontong-Java Plateau; SR, Shatsky Rise.

## 5. Discussion

### 5.1. Carbon-Isotope Segments as Correlation Markers

The  $\delta^{13}\text{C}_{\text{carb}}$  profile of the Cau core, divided into 13 distinct isotope segments, can be correlated in detail with other records worldwide (Figures 4 and 5). This fact provides strong evidence that the  $\delta^{13}\text{C}_{\text{carb}}$  trends and values measured in this hemipelagic outer-shelf succession preserve an original oceanic signature, which makes it suitable for stratigraphic correlation. This is supported by the low correlation between  $\delta^{13}\text{C}_{\text{carb}}$  and  $\delta^{18}\text{O}$  values (Figure 3), which suggests a low diagenetic imprint on C-isotope values (e.g., Jarvis et al., 2011). Although there are many published  $\delta^{13}\text{C}_{\text{carb}}$  Aptian profiles from different basins worldwide, only some of these include detailed biostratigraphic records of calcareous fossils (ammonites, calcareous nannofossils, and/or planktonic foraminifera), and provide the data necessary to test chemostratigraphic correlations based on the informal reference subdivisions of the C-isotope curves of Bottini et al. (2015), Bralower et al. (1999), Herrle et al. (2004), and Menegatti et al. (1998) (Figure 2 and Table SI).

The Cau core record is one of few high-resolution C-isotope records from a continuous expanded section that is well constrained by ammonites from adjacent outcrop (Aguado et al., 1999; Moreno-Bedmar et al., 2012). Its record can be calibrated directly using calcareous nannofossils and planktonic foraminifera and extends from the level of the nannoconid crisis, through the onset of OAE 1a to the lower-upper Aptian boundary, and upwards into the mid—upper Aptian (Figure 4). The lack of well-preserved calcareous fossils is crucial in many sections, and is generally related to low carbonate contents coincident with TOC-rich levels, mostly deposited in deep-ocean pelagic environments, which are otherwise considered to be the best setting to record global stable-isotope signals (Weissert et al., 2008). These settings are also characterized

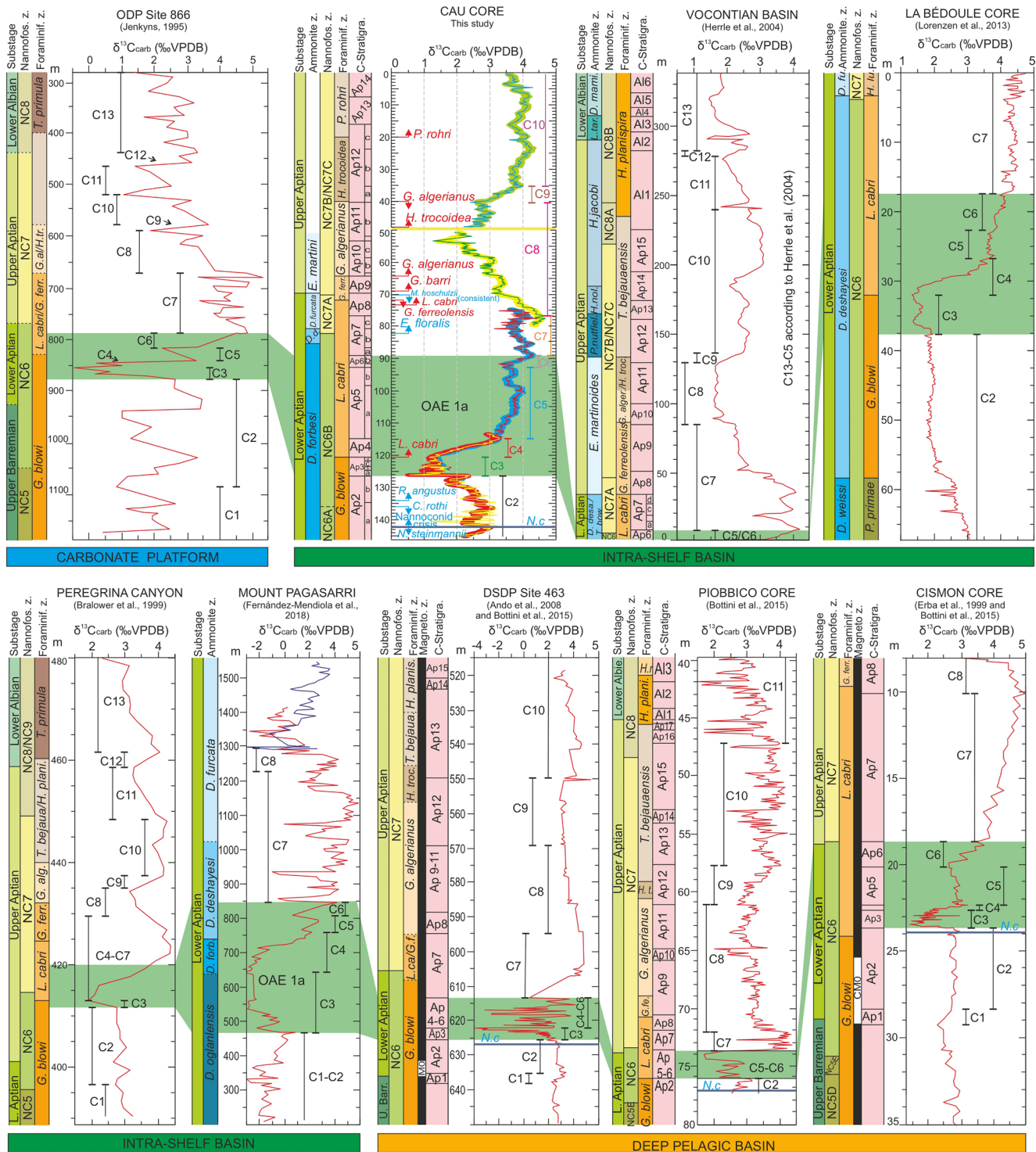


**Figure 5.** Correlation of the Cau core C-isotope stratigraphy with carbonate platform, intrashelf basin, and deep pelagic basin records. Biostratigraphic markers used for calibration: *R. angustus* (*Rhagodiscus angustus*), *L. cabri* (*Leupoldina cabri*), *E. floralis* (*Eprolithus floralis*), *G. ferreolensis* (*Globigerinelloides ferreolensis*), *G. barri* (*Globigerinelloides barri*), *G. algerianus* (*Globigerinelloides algerianus*), *H. trocoidea* (*Hedbergella trocoidea*), and *P. rohri* (*Paraticinella rohri*). For the paleogeographic location of the successions see Figure 4.

by low sedimentation rates leading to thin and sometimes condensed or discontinuous successions and, unfortunately, in many Deep Sea Drilling Project (DSDP), Ocean Drilling Program (ODP), and Integrated Ocean Drilling Program (IODP) sites to an incomplete record.

At the other end of the spectrum, shallow platform records, although generally more expanded, are prone to being affected by early diagenesis and commonly lack biostratigraphically significant open-marine fossils. Some thick coastal successions formed along rapidly subsiding basins serve as good archives for C-isotope stratigraphy (Millán et al., 2009). Intraself basins and distal open platforms accumulating hemipelagic sediments commonly contain thick and continuous successions that preserve a global C-isotope signal (e.g., Fernández-Mendiola et al., 2018; Lorenzen et al., 2013), although their stratigraphy can be affected by local sedimentary conditions and variable subsidence rates. These settings are usually located in rifted margins, where extensional tectonics prevailed during the Aptian at a global scale (e.g., Hay, 2017; Skelton, 2003; Figure 4).

For the correlation of the C-isotope curve, we have selected seven sections with well-characterized C-isotope stratigraphy representing deep pelagic, intrashelf, and shallow-platform settings (Figure 4). These originate from the western Tethys, Central Atlantic, and Pacific oceans and have been widely cited in the literature (see, e.g., data compilations of Erba et al. (2015) and Scott (2016)). An eighth relatively recent record by Fernández-Mendiola et al. (2018) from northern Spain is also included. Table S1 shows a detailed definition of the carbon-isotope stratigraphic units deduced from the analysis of the  $\delta^{13}\text{C}_{\text{carb}}$  profile of the Cau core, their correlation, and biostratigraphic position.

Here, we propose a terminology with 13 C-isotope segments, based on the Cau core data, and their correlation to previous robustly defined segments (Bralower et al., 1999; Bottini et al., 2015; Herrle et al., 2004; Menegatti et al., 1998; Figures 2 and 5). We have followed previous definitions of segments and, where there were differences between them, we have selected the segment boundaries based on the Cau core data and their correlation to other sections. Further subdivisions in some segments are also proposed, which are supported by the high resolution of our data and correlation to previous published records (Figure 2, right column).

Segment Ap2 (C2) is characterized in the Cau core by a lower half with a two-step positive shift of ca. 1‰  $\delta^{13}\text{C}_{\text{carb}}$  followed by a stepped decreasing trend returning back to values around 2‰, which has led to a subdivision into Ap2a and Ap2b (Figure 2).

The base of segment Ap3 (C3) is taken at the most pronounced negative spike in the Cau profile, with a negative shift of 2‰ within a thickness of 0.17 m, embedded in the longer-term decline started with Ap2b subsegment, which also marks the base of the OM-rich interval (ca. 1.2% TOC). This pronounced spike is amplified in the Cau profile because it is preceded and followed by both positive (+0.6‰) and negative (−0.9‰) shifts superimposed on a more gradual falling trend when considering the average long-term profile. An almost identical evolution at the C2–C3 boundary is recorded at Mount Pagasarri in the Basque-Cantabrian Basin of northern Spain (Fernández-Mendiola et al., 2018) and in the Cison core from northern Italy (Bottini et al., 2015), and similar but less marked minima are recorded at the transition between C2 and C3 in other sections, such as La Bédoule in SE France (Lorenzen et al., 2013; Figure 5). Although high-resolution correlation shows differences between sections, the onset of a sharp negative spike is taken as a marker for the base of the Ap3 segment, and hence for the onset of OAE 1a. The documentation of such a marked spike at Cau is likely to be principally a product of the ultrahigh resolution of the data in this part of the core (sample spacing close to 1 cm). This explains why this spike, which is considered to record a major perturbation in the global carbon cycle, is missing in lower resolution profiles, including that obtained for the Cau field section (de Gea et al., 2003; Moreno-Bedmar et al., 2012; Naafs et al., 2016).

The negative excursion and minimum that define the Ap3 segment begin with the negative  $\delta^{13}\text{C}_{\text{carb}}$  “spike” that are observed in several other sections (e.g., DSDP Site 463, Ando et al., 2008; Cison core, Bottini et al., 2015; Menegatti et al., 1998; Figure 5), as well as in  $\delta^{13}\text{C}_{\text{org}}$  records (Basque-Cantabrian Basin, Millán et al., 2009; Carbonero section, Castro et al., 2019). Other differences between sections affecting the Ap3 segment are related to the position of the lowest values of  $\delta^{13}\text{C}_{\text{carb}}$ , which may correspond to the base, middle part or uppermost part of the segment, and also to the definition of the Ap3/C3 segment in each study. This can be related to local factors, such as variable local productivity, and/or secondary effects due

to diagenesis associated with the presence of TOC-rich strata. Nevertheless, the Ap3 segment is a clear negative excursion imposed on a longer-term negative shift, although the resolution of the study and completeness and thickness of the record can compromise the precise placement of its base in less resolved records.

The Ap4 (C4) segment is one of the clearest levels for correlation, as its base is defined by a sharp change toward a positive shift of ca. 2–3‰. In the Cau core, segment Ap4 shows cycles of low amplitude (ca. 0.1‰) that have been also detected in other high-resolution studies (e.g., La Bédoule section, Kuhnt et al., 2011; Pagasarri section, Fernández-Mendiola et al., 2018). The Ap5 (C5) segment represents a distinct interval with overall stable values, and a downwards step in its upper part, generally well expressed in most sections. This is followed by a positive “step” represented by segment Ap6 (C6). Although the Ap5–Ap6 plateau and rise are generally well developed, there are several localities in which segments Ap4–Ap6 cannot be clearly differentiated (e.g., Piobbico core, Site 463, Bottini et al., 2015; Site 398, Li et al., 2008).

Segment Ap7 records a rather noisy  $\delta^{13}\text{C}_{\text{carb}}$  trend with a falling-upwards evolution to a minimum around the middle part of the segment, followed by a prominent positive peak reaching a maximum of 4.7‰ toward the top (Figure 2). Herrle et al. (2004) used the correlative maximum in the Vocontian Basin to mark the top of his Ap7 segment and the top of the interval of high positive  $\delta^{13}\text{C}_{\text{carb}}$  values that characterize the lower Aptian. Menegatti et al. (1998) gave a biostratigraphic dating for the top of segment C7 and base of C8 in the Cison section as the uppermost part of the *L. cabri* Zone close to the base of the *G. ferreolensis* biozone. Bottini et al. (2015) also placed the top of Ap7 at the maximum  $\delta^{13}\text{C}_{\text{carb}}$  values, which correspond to the uppermost part of the *L. cabri* biozone, in both the Cison and Piobbico cores. The maximum of 4.7‰ in the profile of  $\delta^{13}\text{C}_{\text{carb}}$  at Cau provides a clear chemostratigraphic criterion for placing the segment boundary with a very similar biostratigraphic position. It should be emphasized that although chemostratigraphic units are not defined by biostratigraphy, similar to magnetostratigraphy, the latter is essential to provide an independent test of the correlation between sections.

The C8 segment was the uppermost unit defined by Menegatti et al. (1998), being only partly preserved in the Cison section, and exhibits a decrease in  $\delta^{13}\text{C}$  followed by stable values. The unit was subsequently subdivided into segments Ap8 pp. to Ap11 by Herrle et al. (2004). The Cau record depicts the Ap8–Ap11 segments, and inflections in the curve have led to differentiation of additional subdivisions in Ap10 and Ap11 (Figure 2 and Table S1). Although the C8 segment has been widely recognized (e.g., Ando et al., 2008; Bralower et al., 1999; Erba et al., 2015), relatively few studies have utilized the subdivisions of Herrle et al. (2004), though they have been applied in both the Pacific (Site 463, Ando et al., 2008) and Tethyan domains (Piobbico core, Bottini et al., 2015).

Stratigraphically higher C-isotope segments were defined by Bralower et al. (1999) from northeastern Mexico (Peregrina Canyon, Figure 5), and are not present in the Cison core due to a sedimentary gap (Erba et al., 1999). The Cau core records the C9 (positive shift, Ap12a in this study) and C10 (stable values, Ap12b–Ap14 herein, Figure 2) segments, as well as the subdivisions Ap12–Ap14 (Bottini et al., 2015; Herrle et al., 2004). Segments C9–C10 have been recognized worldwide: in the Tethys (Vocontian Basin, Herrle et al., 2004; Piobbico core, Bottini et al., 2015); Central Atlantic (Mazagan Plateau, Herrle et al., 2004); Mexico (Bralower et al., 1999); and recently in the Southern Ocean (Site 511, Falkland Plateau, Dummann et al., 2020), supporting a global correlation for this upper part of the Aptian C-isotope stratigraphy.

## 5.2. Sedimentation Rates

The interval studied in the Cau core embraces most of the Aptian, from the upper part of the *Globigerinellodes blowi* biozone to the lower part of the *Paraticinella rohri* biozone of planktonic foraminifera, NC6A to NC7B–C nannofossils biozones, and Ap2–Ap14 C-isotope segments (Figure 2). Following the chronostratigraphy of Gradstein et al. (2020), this interval corresponds to 120.6–114.2 Ma. Overall sedimentation rates are 2.3 cm/kyr. OAE 1a, represented by Ap3–Ap6, had a duration of 1.0–1.3 Myr (Giraud et al., 2018; Li et al., 2008; Malinverno et al., 2010). Based on these estimates and a thickness of 37.5 m in Cau, the average sedimentation rate for OAE 1a is 2.9–3.7 cm/kyr, slightly higher than the average rate for the complete core. This difference can be explained by changes in accommodation space, as the early Aptian is considered to have higher subsidence rates than the late Aptian, due to a reduction in the intensity of extensional tectonics during the Aptian in the SICM (e.g., Martín-Chivelet et al., 2019, 2002; Vera, 2004). Higher terrigenous

and carbonate inputs fluxes might also have characterized the early Aptian, although the terrigenous:carbonate ratio did not vary significantly from the early to the late Aptian.

The duration of the negative excursion at the onset of OAE 1a (the complete Ap3 segment) has been estimated with significant differences. A short duration of 27–44 kyr (Li et al., 2008) or 22–47 kyr (Malinverno et al., 2010) was originally proposed from the reference Cismon section, whereas longer durations have been calculated from other sites, including >100 kyr from La Bédoule in SE France (Kuhnt et al., 2011; Lorenzen et al., 2013) and >300 kyr for sections in central Turkey and the southern Alps (Hu et al., 2012; Huck et al., 2011). Notably, a revised estimate for the Cismon core indicates an intermediate value of 100–150 kyr, based on a different definition of C3 segment (Bottini et al., 2015). Assuming a duration of between 100 and 300 kyr, the sedimentation rate for Ap3 at Cau is 1.9–5.6 cm/kyr. Segment C4 (Ap4) estimates range between 90 and 239 kyr (Bottini et al., 2015; Malinverno et al., 2010), with a sedimentation rate of 2.4–6.4 cm/kyr. Segment C5 (Ap5) has a duration estimated at 510–570 kyr (Li et al., 2008; Malinverno et al., 2010), which corresponds to a sedimentation rate of 3.7–4.2 cm/kyr. C6 (Ap6) has a duration estimated at 330–350 kyr (Li et al., 2008; Malinverno et al., 2010), this gives a sedimentation rate of 1.2 cm/kyr.

These sedimentation rates lie within error of previous estimates from other sections. Differences are attributable to varying subsidence rates and sediment fluxes, but also to the use of different age models, different definitions of segment boundaries, and factors such as the presence of condensed intervals or discontinuities (Bottini et al., 2015; Castro et al., 2019; Huck et al., 2011; Li et al., 2008; Lorenzen et al., 2013; Malinverno et al., 2010; Scott, 2016).

It is notable that outer-shelf sedimentation along this part of the northern Tethys margin was not affected by increased erosive current activity during the Aptian, as has been observed in numerous northern Tethyan successions of the alpine Tethys (Föllmi et al., 2006). Strong erosive currents related to the Aptian perturbation of the global carbon cycle resulted in the formation of widespread phosphoritic condensation levels (e.g., Föllmi et al., 1994), and a hiatus embracing most of the Aptian in wide sectors of the SICM, where Aptian successions are scarce and located in small fault-bounded depressions (e.g., de Gea et al., 2008; Martín-Chivelet et al., 2019).

### 5.3. Implications for Global Carbon Cycle Perturbations, Climate, and Paleoceanography during the Aptian

Carbonate C-isotope records serve as an excellent tracer for the history of the global carbon cycle (e.g., Arthur et al., 1985; Cramer & Jarvis, 2020; Jenkyns, 2010; Weissert, 1989, 2019). The negative and positive spikes and shifts in the Aptian C-isotope record are linked to changes in  $p\text{CO}_2$  (e.g., Jarvis et al., 2015, 2011; Méhay et al., 2009; Menegatti et al., 1998; Naafs et al., 2016), temperature (e.g., Dumitrescu et al., 2006; Jarvis et al., 2015; Jenkyns, 2018; Kuhnt et al., 2011; Naafs & Pancost, 2016), ocean fertility (e.g., Aguado et al., 2014a, 2016, 2017, 2008; Bottini & Erba, 2018; Bottini et al., 2015; Herrle et al., 2010; Mutterlose & Bottini, 2013), carbonate platform initiation and drowning (e.g., Huck et al., 2011, 2013, 2010; Masse & Fenerci-Masse, 2013; Skelton & Gili, 2012; Skelton et al., 2019) and biotic crises (e.g., nannoconid crisis, Erba, 1994; planktonic foraminiferal and radiolarian turnover, Erbacher & Thurow, 1997; Leckie et al., 2002) or changes in the rudist fauna (Skelton & Gili, 2012). However, despite the dramatic short-term and longer-term shifts recorded in lower Aptian records, no prominent extinction events occurred during the early Aptian, probably due to the increase in the resilience of the Cretaceous biosphere (Weissert, 2019).

Ultimately, changes in the carbon cycle are considered to be related to changes in atmospheric  $\text{CO}_2$  concentrations, particularly due to changes in the volcanic  $\text{CO}_2$  flux resulting from volcanic degassing, methane emissions, and/or metamorphism of carbon-rich deposits (e.g., Jahren et al., 2001; Jenkyns, 2010; Van Breugel et al., 2007; Weissert, 2019; Weissert & Erba, 2004). Excess  $\text{CO}_2$  added to the atmosphere is balanced by its removal through continental weathering and erosion affecting the carbon pump and nutrient supply to the oceans, resulting in enhanced deposition of C-rich sediments, both inorganic and organic, which in turn promotes a reduction in atmospheric  $\text{CO}_2$  concentrations (e.g., Archer, 2010; Jenkyns, 2010; Weissert, 2019). Our new, high-resolution record allows those carbon cycle processes to be revisited.

### 5.3.1. Early Aptian OAE 1a

Segments and subdivisions of the C-isotope curve from the Cau core, correlated worldwide (Figure 5), confirm results from previous studies and further demonstrate the global character of the changes recorded, starting with a major perturbation in the C-cycle corresponding to the OAE 1a (Ap3–Ap6 segments). The first detailed information on the relationship between Aptian C-isotope stratigraphy and global OAE 1a was deciphered more than 20 years ago in the Tethyan pelagic limestone succession at Cismon, NE Italy (Erba et al., 1999; Menegatti et al., 1998). The Cismon section (Figure 5) preserves the sedimentary record of OAE 1a represented by the “Livello Selli” (Coccioni et al., 1987; Wezel, 1985) at outcrop and in a drill core. Both drill core and outcrop provide a distinct pattern of change in the carbonate and organic C-isotope curves, starting with a prominent “negative spike” and followed by a positive C-isotope excursion. The negative spike “C3” in the C-isotope curves generated by Menegatti et al. (1998) marks the base of the geochemically defined OAE 1a and is coincident with the base of an interval displaying an increased incidence of “black shale” (TOC > 1 wt%) and organic-rich marl (TOC 0.5–1 wt%) interbeds. The transition to low C-isotope values in carbonate carbon, in organic carbon, and in marine and terrestrial biomarkers (Méhay et al., 2009; Naafs et al., 2016) has been interpreted as evidence for the sudden addition of large quantities of isotopically light carbon from volcanic CO<sub>2</sub> sources and, possibly, from oxidized methane derived from gas hydrates (Adloff et al., 2020; Jähren et al., 2005; Méhay et al., 2009; Weissert & Erba, 2004), or to sill intrusions into marine organic-rich sediments (Polteau et al., 2016).

The addition of huge amounts of carbon dioxide triggered disturbances in climate and oceanography. The transition to low C-isotope values at the base of OAE 1a was accompanied by an increase in seawater temperatures in the Boreal realm, the Central Atlantic, and the Pacific oceans (Dumitrescu et al., 2006; Mutterlose et al., 2014; Naafs & Pancost, 2016; O’Brien et al., 2017). Temperature variations were coupled with paleoceanographic perturbations as reflected by repeated deposition of organic-carbon-rich sediments (exemplified by the “Livello Selli”) in basinal and shallow marine settings (Atlantic-Tethys, e.g., Aguado et al., 2014a; Castro et al., 2019; Coccioni et al., 2006; de Gea et al., 2008; Giorgioni et al., 2015; Lorenzen et al., 2013; Menegatti et al., 1998; Millán et al., 2009; Quijano et al., 2012) and on submarine highs (Pacific, e.g., Ando et al., 2008; Dumitrescu & Brassell, 2005; Jenkyns, 1995). Conditions were favourable for widespread deposition of “black shales” during the OAE 1a which had a duration of around 1–1.3 Myr (Giraud et al., 2018; Li et al., 2008; Malinverno et al., 2010, 2012).

There is an ongoing controversy on the pattern of environmental change that occurred at the beginning of OAE 1a. In the Cau core, C-isotope variations in the lower part of Ap2 (Ap2a), from 135 to 142 m, are considered to be probably related to diagenetic alteration linked to weathering, evidenced by coupling of  $\delta^{13}\text{C}_{\text{carb}}$  and  $\delta^{18}\text{O}$  values and by a poor preservation of calcareous nannofossils and planktonic foraminifera, possibly caused by the recrystallization of the carbonates induced by fluid flow along a nearby fracture or fault affecting core D4. Nevertheless, the five point-average profile of Ap2a shows steady values of  $\delta^{13}\text{C}_{\text{carb}}$  close to 2.6‰ (Figures 2 and 6), similar to other sections (e.g., Cismon, Peregrina Canyon, DSDP Site 463; Figure 5). The Ap2b and Ap3 segments record a general negative shift of ca. 2.6‰ in  $\delta^{13}\text{C}_{\text{carb}}$  with a complex evolution made up of a succession of up to seven negative peaks (Figures 2 and 6). These peaks record rapid positive shifts of 0.3–1.5‰, suggesting a multiphase evolution in the accumulation of  $\delta^{13}\text{C}$  depleted carbon in the atmosphere-ocean system. Similar patterns are also evident in other highly resolved  $\delta^{13}\text{C}_{\text{carb}}$  records, as at Cismon (Bottini et al., 2015), ODP Site 866 (Jenkyns, 1995), Mount Pagasarri (Fernández-Mendiola et al., 2018), DSDP Site 463 (Ando et al., 2008; Bottini et al., 2015) (Figure 5), and Pusiano (Giorgioni et al., 2015), as well as in  $\delta^{13}\text{C}_{\text{org}}$  records (Carbonero, Castro et al., 2019; El Pui, Sánchez-Hernández & Maurrassé, 2016). These variations in the C-isotope profile could be related to changes in the intensity of the volcanic activity in the Ontong-Java Plateau. However, recent studies on high-resolution records have led to the differentiation of successive phases within the onset of OAE 1a, with both volcanic CO<sub>2</sub> and methane emissions (Adloff et al., 2020; Bottini et al., 2012, 2015; Erba et al., 2010; Méhay et al., 2009). The largest negative spike in the Cau core has an amplitude of –1.8‰ and an estimated duration of <10 kyr. Such a rapid shift is consistent with organic carbon and/or methane emissions, more <sup>13</sup>C-depleted than volcanic CO<sub>2</sub> (e.g., Wagner et al., 2007).

Méhay et al. (2009) and Erba et al. (2010) documented a succession of C-depleted pulses (of CO<sub>2</sub> and CH<sub>4</sub>) during the onset of OAE 1a (Figure 6). Warming and destabilization of methane hydrates were considered

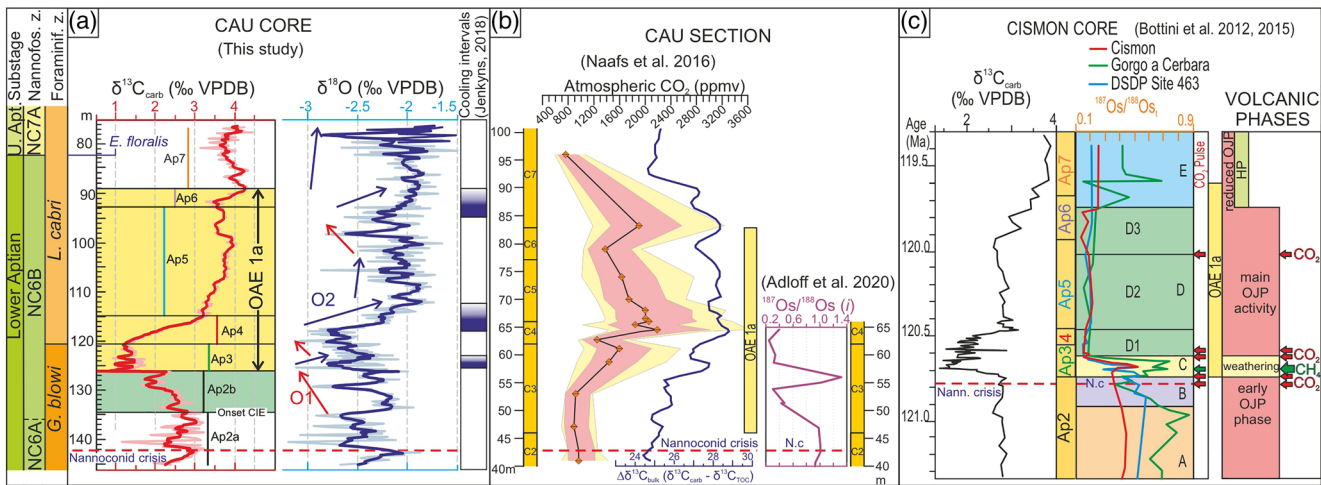


**Figure 6.** (a) Early Aptian C and O-isotope stratigraphy of the Cau core, and cooling intervals from Jenkyns (2018). (b) Previous records from the Cau field section:  $\text{pCO}_2$  estimates from Naafs et al. (2016); Os-isotope data from Adloff et al. (2020). (c) C- and Os-isotope data from Cision core (Bottini et al., 2012, 2015), with Os-isotope segments A to E Gorgo a Cerbara data from Tejada et al. (2009). Volcanic phases from Bottini et al. (2012), with  $\text{CO}_2$  and  $\text{CH}_4$  pulses (right) from Erba et al. (2010) and Méhay et al. (2009).

as a trigger for the  $\text{CH}_4$  pulse (Interval IV of Méhay et al., 2009). This injection of  $\text{CH}_4$  possibly initiated a short interval of warming and subsequent accelerated weathering rates (Bottini et al., 2012), documented by a short-lived ( $\sim 100$  kyr) osmium-isotope excursion to radiogenic compositions (Adloff et al., 2020; Bottini et al., 2012; Tejada et al., 2009). Increased weathering during OAE 1a is also indicated by calcium isotopes (Blattler et al., 2011) and lithium isotopes (Lechler et al., 2015). The Os-isotope record from the Cau outcrop section (Adloff et al., 2020) shows this episode of enhanced weathering (positive  $^{187}\text{Os}/^{188}\text{Os}_i$  spike, Figure 6), which postdates the prominent negative peak in  $\delta^{13}\text{C}$  (base of Ap3 segment, Figure 6). This may be consistent with the correlation of the C-isotope spike and the  $\text{CH}_4$  pulse postulated by Méhay et al. (2009; Figure 6) even if resolution of the Os-isotope curve at Cau is very low.

Carbon cycle modelling from the Cau outcrop section (Adloff et al., 2020) proposed a dominance of methane sources for the carbon emissions during the onset of OAE 1a, which contrasts with the biomarker-based interpretation of the carbon source by Méhay et al. (2009). Kemp et al. (2005) reported a very similar C-isotope pattern from the Toarcian OAE, with a succession of abrupt negative peaks in  $\delta^{13}\text{C}$ , which were interpreted as the result of pulses of methane emissions controlled by astronomically forced changes in climate, superimposed upon longer-term global warming. Similar responses of the climate system to rapid increases in atmospheric carbon with acceleration of the hydrological cycle have been postulated for other OAEs (e.g., Van Helmond et al., 2013).

The multiphase character of the complete negative C-isotope excursion possibly resulted from the interaction of volcanism, methane emissions, and the complex interplay of feedback mechanisms, particularly continental weathering, organic matter and carbonate burial, and carbon dioxide drawdown. Evidence for a short-term and rapid shallowing of the CCD is documented at the base of OAE 1a at Cision (Erba et al., 2010). Shallowing of the CCD contributed to neutralization of excess  $\text{CO}_2$  in atmosphere and oceans.

Interestingly, the neighbouring shallow-water carbonate platform area recorded a demise coeval with the onset of OAE 1a, followed by deposition of siliciclastics, which is interpreted as the result of an abrupt environmental perturbation (Castro et al., 2008; Skelton et al., 2019). Biostratigraphic and C-isotope data (Skelton et al., 2019) are consistent with a correlation between the major negative shift in  $\delta^{13}\text{C}$  recorded in the Cau core and the demise of the platform. These observations agree with data published from the Basque-Cantabrian basin (Millan et al., 2009, 2011). The subsequent deposition of siliciclastics on the platform settings, could represent the local response to global enhanced weathering (Blattler et al., 2011; Erba et al., 2010; Lechler et al., 2015; Méhay et al., 2009; Tejada et al., 2009). Demise of carbonate platforms and carbonate ramps along the northern Tethys coincided with OAE 1a and a widespread nannoconid crisis (Erba et al., 2004). These changes have been considered to be related to surface ocean acidification due to

increased  $p\text{CO}_2$  during OAE 1a (e.g., Erba et al., 2010; Skelton & Gili, 2012; Wissler et al., 2003), although this is a matter of debate (Gibbs et al., 2011; Naafs et al., 2016). The Cau core record confirms that the nanconid crisis predates the OAE 1a, as has also been recorded in Cison, and correlated to a volcanic pulse (Bottini et al., 2015; Erba et al., 2010).

The principal consequence of an increase in atmospheric  $\text{CO}_2$  during the onset of OAE 1a was global warming (e.g., Erba et al., 2015; Jenkyns, 2010). Previous  $p\text{CO}_2$  reconstructions from the onset of OAE 1a at Cison (Méhay et al., 2009), based on biomarkers, suggest intense volcanic activity near the base of the Selli Level, followed by a short event of doubling of  $p\text{CO}_2$ . A  $p\text{CO}_2$  reconstruction from the Cau outcrop section, based on compound-specific and bulk  $\delta^{13}\text{C}_{\text{carb}}$  (Naafs et al., 2016), indicates a  $p\text{CO}_2$  increase during the negative CIE starting around 800–1,000 ppm, then reaching maximum values of  $2,000 \pm 1,200$  ppm before the recovery of the negative CIE (Figure 6). Temperature records for OAE 1a have been derived from multiple proxies ( $\text{TEX}_{86}$ , oxygen isotopes, and nannofossil indices) (e.g., Aguado et al., 2014a; Bottini et al., 2015, 2018; Kuhnt et al., 2011; Naafs & Pancost, 2016; O'Brien et al., 2017; Steinig et al., 2020). The onset of OAE 1a was characterized by an increase in temperature of 2–5 °C (e.g., Bottini et al., 2015; Naafs & Pancost, 2016), with highest temperatures coinciding with the most negative C-isotope values. A first transient episode of cooling within OAE 1a has been documented (Bottini et al., 2015; Hu et al., 2012; Jenkyns, 2018; Naafs & Pancost, 2016), that correlated with the interval of increased weathering (interval IV of Méhay et al., 2009) referred to above. This episode could correspond to a brief positive trend in  $\delta^{18}\text{O}$  during Ap3 (or Ap3b) (Figure 6).

The foremost geochemical signatures recorded in ocean deep environments are also clearly documented in the intrashelf settings where the Cau succession was deposited, suggesting efficient active oceanic circulation during the early Aptian. This efficient circulation in the Cau area was probably favoured by its paleogeographic location, along the seaway between the Tethys and Central Atlantic (Figure 4), together with a rising sea-level episode (e.g., Castro et al., 2008; Haq, 2014; Martín-Chivelet et al., 2019; Maurer et al., 2013). Enhanced shelf-circulation during the Aptian has been noted in other parts of the northern margin of the Tethys, with development of condensed sedimentation on drowned carbonate ramps (e.g., Föllmi et al., 2006; Wissler et al., 2003).

Segment Ap4 represents a major shift to positive C-isotope values and is coeval to widespread organic matter deposition in marine environments (see Section 5.4), likely driving the positive carbon-isotope shift and drawing down  $\text{CO}_2$ . Consistent with this, Ap4 is associated with a second transient cooling of 3–6 °C (Bottini et al., 2015; Dumitrescu et al., 2006; Hu et al., 2012; Jenkyns, 2018; Kuhnt et al., 2011; Naafs & Pancost, 2016; Stein et al., 2012). Oxygen isotopes in the Cau core show a positive step in the middle part of Ap4 to the base of Ap5 segments (Figure 6) that could reflect a cooling interval, coeval to a distinct drop in  $p\text{CO}_2$  documented from the Vocontian Trough (Heimhofer et al., 2004) and from the Cau section (Naafs et al., 2016; Figure 6). Os-isotope data indicate that volcanism remained active with no variations across the C4/Ap4 segment (Bottini et al., 2012; Tejada et al., 2009), suggesting that continued  $\text{CO}_2$  emissions were outpaced by carbon drawdown, resulting in a drop in  $p\text{CO}_2$  and temperatures (Jenkyns, 2018; Figure 6a).

The later part of OAE 1a (Ap5–Ap6 segments) represents the longer C-isotope positive plateau, lasting ca. 900 kyr, that records an overall stability in the C and O isotopes in the Cau core and in records worldwide (e.g., Erba et al., 2015; Jenkyns, 2010, 2018; Figures 5 and 6), suggesting no major perturbations in the carbon cycle during this long-lasting interval. Os-isotope data indicate active volcanism (Bottini et al., 2012; Tejada et al., 2009), and the absence of evidence for enhanced weathering (e.g., Blattler et al., 2011; Lechler et al., 2015) would suggest that there was a balance between volcanic  $\text{CO}_2$  emissions and carbon drawdown. Overall cooler temperatures than previous characterize this interval (e.g., Bottini et al., 2015; Jenkyns, 2010), whereas a third transient cooling episode across the Ap5/Ap6 boundary has been recorded in several sections (Bottini et al., 2015; Dumitrescu et al., 2006; Hu et al., 2012; Jenkyns, 2018). This cooling episode could correspond to a positive step in oxygen isotopes in the Cau core (Figures 2 and 6) and to a drop in  $p\text{CO}_2$  (Figure 6; Naafs et al., 2016).

The transition to Ap7 segment records the end of global anoxia-dysoxia (e.g., Erba et al., 2015), that is reflected in Cau by a gradual disappearance of the organic-rich laminated facies that were frequent in the OAE 1a interval (facies type 1, Figure 2). This transition coincided with the end or reduction of the main

volcanic episode of the Ontong-Java Plateau (Bottini et al., 2012; Tejada et al., 2009) and a prominent global cooling (Bottini et al., 2015; Naafs & Pancost., 2016; O'Brien et al., 2017). Oxygen isotopes in the Cau core do not show any significant shift at this transition, although the high scatter of data in this interval likely indicates that they have been affected by diagenetic alteration. Nevertheless, the  $p\text{CO}_2$  record drops back to pre-OAE values during Ap6 and Ap7 (Heimhofer et al., 2004; Naafs et al., 2016; Figure 6). Although the top of Ap6 is generally considered as the end of OAE 1a, the Ap7 segment records a gradual return to pre-OAE conditions, and has been considered as the “recovery stage” (Hu et al., 2020), affected by protracted environmental perturbations (Castro et al., 2019). The upper part of Ap7 segment records the highest C-isotope values of the core, which mark the end of the positive plateau, and the initiation of a decreasing trend that characterizes the base of the upper Aptian.

### 5.3.2. The Late Aptian

The upper Aptian records a long-term negative-positive C-isotope excursion, with a large amplitude of ca. 2–3‰. Oxygen isotopes of the Cau core through this interval present overall stable values of ca. 1.8‰, consistent with cooler temperatures than those of the early Aptian, which is in agreement with previous studies (e.g., Bottini & Erba, 2018; O'Brien et al., 2017; see following discussion). The Ap8–Ap10 segments define a pulsed negative C-isotope evolution, followed by a stepwise positive trend within segments Ap11 to Ap12 (Figure 2). This C-isotope excursion is recorded with variable amplitudes in the Mediterranean Tethys (e.g., Piobacco core; Bottini et al., 2015; Vocontian Basin, Herrle et al., 2004; Figure 5; central Italy, Raspini, 2012; Prebetic Platform, Castro et al., 2014; Basque-Cantabrian basin, Millán et al., 2014), Central Atlantic (Peregrina Canyon, Bralower et al., 1999), and the Pacific (ODP Site 866; Jenkyns, 1995).

The highest TOC concentrations in the Cau core, with the presence of several levels of laminated facies (Facies type 1, Figure 2) are recorded within the low upper Aptian excursion interval, which correlates to the black shales of the “Niveau Fallot” in the Vocontian Basin (Friedrich et al., 2003; Herrle et al., 2004). Nevertheless, this negative excursion is not associated with widespread organic-rich deposits, which are recorded only at a regional scale, as in the Vocontian Basin (Brehéret, 1988; Friedrich et al., 2003; Herrle et al., 2004), the Prebetic Platform (Cau core and Sierra Mariola, Castro et al., 2014), and, with less precise dating, in the Pacific (Arthur et al., 1990). Friedrich et al. (2003) interpreted the upper part of the “Niveau Fallot” as having been deposited during a drop in sea level, which reduced the ocean circulation within the Vocontian Basin. A similar model could be applied to the Cau core area, probably affected by the global sea-level fall that occurred at the beginning of the negative C-isotope excursion at Ap9 (e.g., Maurer et al., 2013; Millán et al., 2014). Leckie et al. (2002) considered the peak of the negative CIE at Ap10–Ap11 as a possible OAE, based on its global expression and associated records of black shales.

Volcanic degassing from the late stages of the greater Ontong-Java event and early phases of the Southern Kerguelen Plateau (Erba et al., 2015; Frey et al., 2003; Timm et al., 2011) could have been responsible for the Ap8–Ap10 negative C-isotope trend. This interval recorded global warming (Bottini et al., 2015; McAnena et al., 2013), although with cooler temperatures than in the early Aptian. The stepwise negative evolution of the C-isotope profile in Cau core could be linked to pulses in the volcanic activity, although these are not well defined in other records (Figure 5). The duration of the Ap8–Ap10 interval is ca. 1.5 Myr (based on Gradstein et al. (2020)). This implies that, although the amplitude of this C-isotope excursion is similar to that of the CIE of the OAE 1a, the perturbation in the global carbon cycle was more gradual.

The Ap11–Ap12 segments record a positive shift of similar amplitude (ca. 3‰) and duration (ca. 1.5 Myr according to Gradstein et al. (2020)) than the previous negative trend. This interval is considered to be coeval to the volcanism associated with Kerguelen Plateau Large Igneous Province (LIP) volcanism, of subaerial character (Bottini & Erba, 2018; Erba et al., 2015), which could have caused ash emissions and cooling (Bottini et al., 2015; Erba et al., 2015). The initiation of the latest Aptian cool snap is considered to start at the Ap10 segment, with a second pulse at the Ap12 (Bottini & Erba, 2018; Bottini et al., 2015; Maurer et al., 2013; McAnena et al., 2013). A high rate of C-isotope change is recorded in the Ap12-a segment (Millan et al., 2014; equivalent to C9 segment of Bralower et al., 1999; Figure 2), with ca. +1.5‰  $\delta^{13}\text{C}_{\text{carb}}$ , which has been recorded in several marine settings (Figure 5). The positive excursion has also been recorded from terrestrial environments where it is thought to be coeval to a major episode of global change with intense aridification in North America (Lugvidson et al., 2015); it also correlates to an interval of accelerated global weathering based on Li-isotopes (Lechler et al., 2015). In the absence of widespread organic matter

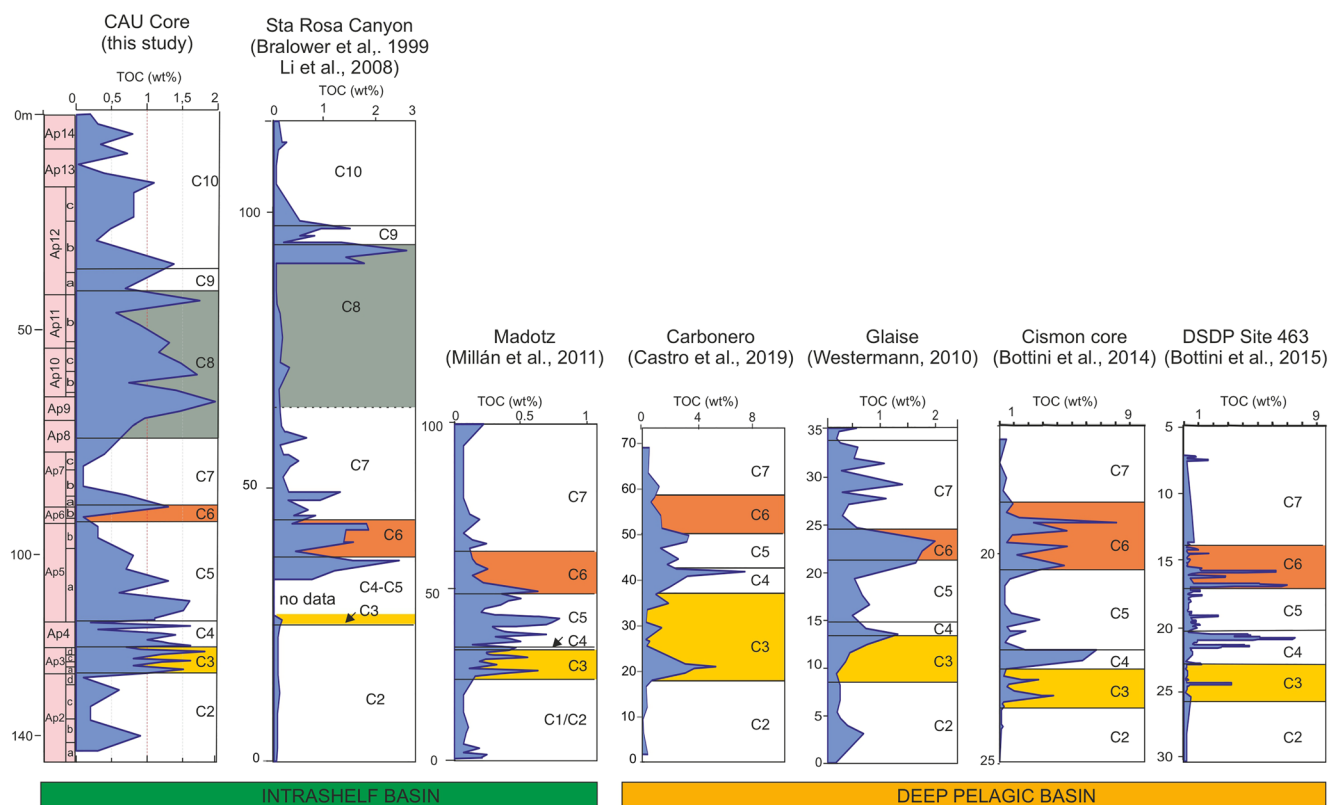


**Figure 7.** Comparison of the TOC content in different sections worldwide deposited in intrashelf basins and deep pelagic basins. For location of the sites see Figure 4. TOC, Total Organic Carbon.

deposition during this time, the positive CIE probably was the result of the increased weathering and subsequent carbon drawdown (e.g., Jenkyns, 2010, 2018).

The uppermost part of the Cau core (Ap13–Ap14) records high values of  $\delta^{13}\text{C}_{\text{carb}}$ , coeval to globally cool temperatures (Bottini & Erba, 2018; McAnena et al., 2013; Millán et al., 2014; Mutterlose et al., 2009; Weissert & Lini, 1991) prior to the deposition of the overlying shallow carbonate platform of the Seguilí Formation, representing a progradational episode linked to a relative sea-level fall (Castro et al., 2008). Interestingly, McAnena et al. (2013) highlighted a brief high thermal episode (HTE) in the middle part of the Ap14 segment, that might correlate with the initiation of the shallow carbonate platform in Cau.

#### 5.4. TOC Distribution and Comparison With Other Basins

Although globally there was widespread deposition of marine OM during OAE 1a, TOC concentrations in sediments are considered to have been strongly affected by local conditions, and therefore they have not been generally used for detailed correlation (e.g., Jenkyns, 2010). Nevertheless, there is a link between OM deposition and C-isotope records, as positive peaks in  $\delta^{13}\text{C}$  are considered to be largely a response to the increased burial of OM at a global scale, removing isotopically light carbon from the oceanic and atmospheric reservoirs. This is the classic explanation for positive  $\delta^{13}\text{C}$  excursions accompanying OAEs (e.g., Erba et al., 2015; Jenkyns, 2010; Kump & Arthur, 1999; Scholle & Arthur, 1980; Weissert, 2000).

The correlation between chemostratigraphy and TOC enrichments is key to understand perturbations in the carbon cycle during OAEs (e.g., Arthur et al., 1990; Bottini et al., 2015; Menegatti et al., 1998). We have attempted a comparison between TOC enrichments and C-isotope segments using well-calibrated records based on a robust C-isotope stratigraphy. We have selected sections from intrashelf basinal and deep pelagic settings from the Tethys, Pacific and Mexico (Figures 4 and 7). Most of the records are focused on OAE 1a,

extending from segment C1 to C7, whereas the Santa Rosa Canyon spans the same stratigraphic interval as the Cau core (Ap2–Ap14 or C2–C10).

The correlation (Figure 7) shows that, although there are differences among sites that affect TOC concentrations and their detailed vertical evolution, some general common patterns persist: (1) the first interval of TOC enrichment coincides generally with the base or lower part of segment C3 at the onset of OAE 1a; (2) the second enrichment level occurs within segment C4, coincident with steeply rising  $\delta^{13}\text{C}_{\text{carb}}$  values; (3) a third episode of enhanced organic matter deposition within OAE 1a took place generally earlier in intrashelf basins, lying within segment C5, whereas the highest concentrations of TOC in deep pelagic basins occur in segment C6. Segment C7, postdating OAE 1a, generally shows low TOC contents, and later enrichments probably have only a local or regional extent. Notably, the thick interval of high TOC values characterizing the upper Aptian C8–lower C10 segments at Cau (Ap9–Ap13) is not seen at Santa Rosa Canyon, where TOC contents remain low through most of C8 and a second large TOC peak is confined to a short interval spanning the top of C8 and C9. This further highlights the regional nature of organic carbon preservation.

The comparison between C-isotope and TOC records promotes discussion on their link to global carbon cycling. The first episode of TOC enrichment coincides with the negative excursion at the onset of OAE 1a, considered to reflect a sharp input of light carbon into the atmosphere, either from volcanic and/or methane sources (e.g., Adloff et al., 2020; Méhay et al., 2009; Weissert, 2000). The consequent increase in temperatures could have resulted in an intensification of the hydrological cycle, increased terrestrial weathering and runoff, enhanced upwelling and ocean fertilization leading to a productivity-driven episode of OM accumulation (e.g., Bottini et al., 2012; Castro et al., 2019). The second episode of TOC enrichment occurred in the opposite scenario, coeval to sharply rising  $\delta^{13}\text{C}$  (C4 segment). This interval has been explained as the result of widespread deposition of OM leading to increased accumulation of isotopically light carbon in marine sediments, with a consequent increase in  $\delta^{13}\text{C}$  values in marine and atmospheric reservoirs (e.g., Bottini et al., 2015; Jenkyns, 2010; Weissert, 2000).

Interestingly, the third episode of TOC enrichment seems to be diachronous, taking place earlier in intrashelf basins (C5) and later in deep pelagic basins (C6), where C5 is represented by low TOC contents (Figure 7). This might be related to eutrophication from terrestrial inputs mostly affecting continental margins during C5, with the subsequent establishment of anoxia in deep marine basins during the C6 segment, as suggested by increases in OM deposition in deep marine environments during this interval (Figure 7), and proposed by Castro et al. (2019) based on biomarker evidence. A shift from enhanced productivity to enhanced preservation across OAE 1a has also been proposed by previous studies on western Tethys sections (Bottini & Erba, 2018; Castro et al., 2019; Westermann et al., 2013). A possible explanation for this evolution is a reduction in the oxygenation of deep marine waters, due to the oxidation of OM. Widespread deposition of OM may occur when a threshold related to the balance between productivity and organic matter oxidation is crossed (Robinson et al., 2004). This difference can also account for the stability in the  $\delta^{13}\text{C}$  values through C5, as a global reduction in OM deposition could have led to an outpacing of  $\text{CO}_2$  volcanic inputs during this interval (e.g., Bottini et al., 2012; Tejada et al., 2009), also related to an intensification of the oceanic thermohaline circulation (Menegatti et al., 1998).

Above OAE 1a, the TOC increase observed locally in segment Ap9 has been correlated to the “Niveau Fallot” defined in the Vocontian Basin (e.g., Herrle et al., 2004), probably indicating an episode of regional-scale organic matter burial (see discussion in Section 5.3.2). At a global scale, after OAE 1a, temperatures, and  $\text{CO}_2$  concentrations fell during the later Aptian, and episodes of ocean fertilization have been linked to ash dispersion from subaerial volcanism, but no prominent episodes of anoxia occurred during the remainder of the Aptian (Erba et al., 2015). Bottini and Erba (2018) demonstrated that temperature and fertility were mostly independent from each other during the Aptian, with the exception of the onset of OAE 1a, when there was an increase in both parameters.

## 6. Conclusions

Our high-resolution  $\delta^{13}\text{C}_{\text{carb}}$  record from the Cau core is proposed as a new global reference from a shelf setting for stratigraphic correlation of the lowermost Aptian to the mid-upper Aptian, including OAE1a, due to its expanded character, the continuity of the record, and the robust preservation of geochemical and biostratigraphic signals.

The combination of C-isotope stratigraphy and integrated biostratigraphy provides a very high stratigraphic resolution (0.5–11 kyr), which has permitted the recognition of previously defined C-isotope segments and the subdivision of some of these into subunits with potential for improved correlation to sections worldwide. Crucially, detailed correlation based primarily on  $\delta^{13}\text{C}_{\text{carb}}$  records and calibrated using biostratigraphic markers demonstrates that the C-isotope record from Cau predominantly reflects a global signal and therefore provides a robust basis for further paleoenvironmental and paleobiologic analyses at high temporal resolution.

The C-isotope record of the onset of OAE 1a in the Cau core is characterized by a long-term decline in C-isotope values. The analysis at ultrahigh resolution reveals a succession of marked negative C-isotope peaks, probably linked to pulses in volcanism and/or methane emissions. The major ( $-1.8\%$ ) short-term (<10 kyr) shift in the C-isotope record marks the base of OAE 1a (base of C3/Ap3 segment; e.g., Erba et al., 1999; Menegatti et al., 1998), and the beginning of the deposition of organic-rich deposits. This ultrahigh-resolution record is in agreement with observed patterns in pelagic sections, and provides new insights into the processes and rates of perturbations to the global carbon cycle.

Late OAE 1a records a rapid shift to high C-isotope values (Ap4), probably related to widespread deposition of organic-rich sediments, resulting in a cooling episode, followed by a long-term episode of general stability (Ap5–Ap6) that could represent a balance between volcanic  $\text{CO}_2$  degassing and carbon drawdown.

The upper Aptian displays a remarkable long-lasting negative-positive C-isotope excursion of global character. The negative trend (Ap8–Ap10 segments) was coeval to a phase of submarine volcanism and reflected in increased regional accumulation of organic-rich deposits. Nevertheless, this isotope excursion is not related to major global climate perturbations, probably due to their slow rates of change, with the exception of a rapid C-isotope negative step during Ap9, which was probably coeval to a brief episode of global change. The subsequent positive trend (Ap11–Ap14) was coeval to globally cool temperatures, and records a gradual reduction in the TOC accumulation in Cau.

TOC distributions in the Cau core and correlation with well-characterized records at a global scale have revealed that, beyond local controls, there are common ocean-wide patterns in the stratigraphy of organic-rich levels, which are strongly controlled by changes in the global carbon cycle. The stratigraphic distribution of TOC through OAE 1a indicates that specific time intervals of globally enhanced OM deposition are generally coeval to periods of rapidly changing  $\delta^{13}\text{C}$  values, but some regional diachroneity is apparent, whereas intervals with stable  $\delta^{13}\text{C}$  values coincide with phases of less OM deposition. This provides evidence for the importance of OM burial as a feedback mechanism in response to increased carbon inputs into the ocean-atmosphere system.

## Data Availability Statement

Data available online at: <https://doi.org/10.1594/PANGAEA.920558>.

## References

- Adloff, M., Green, S. E., Parkinson, I. J., Naafs, B. D. A., Preston, W., Ridgwell, A., et al. (2020). Unraveling the sources of carbon emissions at the onset of Oceanic Anoxic Event (OAE) 1a. *Earth and Planetary Science Letters*, 530, 1–9. <https://doi.org/10.1016/j.epsl.2019.115947>
- Aguado, R., Castro, J. M., Company, M., & de Gea, G. A. (1999). Aptian bioevents—An integrated biostratigraphic analysis of the Almadich Formation, Inner Prebetic Domain, SE Spain. *Cretaceous Research*, 20, 663–683. <https://doi.org/10.1006/cres.1999.0176>
- Aguado, R., Company, M., Castro, J. M., de Gea, G. A., Molina, J. M., Nieto, L. M., & Ruiz-Ortiz, P. A. (2018). A new record of the Weissert episode from the Valanginian succession of Cehegin (Subbetic, SE Spain): Bio- and carbon isotope stratigraphy. *Cretaceous Research*, 92, 122–137. <https://doi.org/10.1016/j.cretres.2018.07.010>
- Aguado, R., de Gea, G. A., Castro, J. M., O'Dogherty, L., Quijano, M. L., Naafs, B. D. A., & Pancost, R. D. (2014a). Late Barremian–early Aptian dark facies of the Subbetic (Betic Cordillera, southern Spain): Calcareous nannofossil quantitative analyses, chemostratigraphy

## Acknowledgments

The authors wish to express special thanks to the municipality of Llíber (Alicante) and its mayor, D. José Juan Reus, who provided us with all kinds of facilities for carrying out the drilling. Javier Jáimez and Emilio Peñalver, the two technicians, who conducted the drilling are also acknowledged. David Gallego-Torres greatly contributed with the sampling and description of the cores. This work has been funded by the Spanish Government, Ministry of Science and Technology (research project CGL2014-55274-P), Research Group RNM-200 (Junta de Andalucía), and University of Jaén (FEDER-UJA 1265149). Laboratory technicians A. Piedra, A. Carrillo, M. J. Campos, and Inés Sanchís are acknowledged for their help in processing of micropaleontology samples and technical support. Support from Equinor (formerly Statoil) research contract 4502299156 to I. Jarvis is gratefully acknowledged. The authors are very grateful to Elisabetta Erba and R. Mark Leckie, whose constructive comments led to significant improvements in the final version of this paper, and to Ursula Röhl and Matthew Huber for their helpful editorial assistance.

- and paleoceanographic reconstructions. *Palaeogeography, Palaeoclimatology, Palaeoecology*, 395, 198–221. <https://doi.org/10.1016/j.palaeo.2013.12.031>
- Aguado, R., de Gea, G. A., & O'Dogherty, L. (2014b). Integrated biostratigraphy (calcareous nannofossils, planktonic foraminifera, and radiolaria) of an uppermost Barremian–lower Aptian pelagic succession in the Subbetic Basin (southern Spain). *Cretaceous Research*, 51, 153–173. <http://dx.doi.org/10.1016/j.cretres.2014.06.002>
- Aguado, R., O'Dogherty, L., & Sandoval, J. (2008). Fertility changes in surface waters during the Aalenian (mid Jurassic) of the western Tethys as revealed by calcareous nannofossils and carbon-cycle perturbations. *Marine Micropaleontology*, 68, 268–285.
- Aguado, R., O'Dogherty, L., & Sandoval, J. (2017). Calcareous nannofossil assemblage turnover in response to the Early Bajocian (Middle Jurassic) palaeoenvironmental changes in the Subbetic Basin. *Palaeogeography, Palaeoclimatology, Palaeoecology*, 472, 128–145. <https://doi.org/10.1016/j.palaeo.2017.01.044>
- Aguado, R., Reolid, M., & Molina, E. (2016). Response of calcareous nannoplankton to the Late Cretaceous Oceanic Anoxic Event 2 at Oued Bahloul (central Tunisia). *Palaeogeography, Palaeoclimatology, Palaeoecology*, 459, 289–305. <http://dx.doi.org/10.1016/j.palaeo.2016.07.016>
- Ando, A., Huber, B. T., & Premoli Silva, I. (2013). *Paraticinella rohri* (Bolli, 1959) as the valid name for the latest Aptian zonal marker species of planktonic foraminifera traditionally called *bejaouaensis* or *eubejaouaensis*. *Cretaceous Research*, 45, 275–287. <https://doi.org/10.1016/j.cretres.2013.05.002>
- Ando, A., Kaiho, K., Kawahata, H., & Kakegawa, T. (2008). Timing and magnitude of early Aptian extreme warming: Unraveling primary  $\delta^{18}\text{O}$  variation in indurated pelagic carbonates at Deep Sea Drilling Project Site 463, central Pacific Ocean. *Palaeogeography, Palaeoclimatology, Palaeoecology*, 260, 463–476. <https://doi.org/10.1016/j.palaeo.2007.12.007>
- Archer, D. (2010). *Global carbon cycle*. Princeton Primers in Climate (p. 214). Princeton, NJ: Princeton University Press. Retrieved from <https://press.princeton.edu/books/paperback/9780691144146/the-global-carbon-cycle>
- Arthur, M. A., Dean, W. E., & Schlanger, S. E. (1985). Variations in the global carbon cycle during the Cretaceous related to climate, volcanism and changes in atmospheric  $\text{CO}_2$ . The carbon cycle and atmospheric  $\text{CO}_2$ : Natural variations Archean to present. *Geophysical Monograph Series*, 32, 504–530.
- Arthur, M. A., Jenkyns, H. C., Brumsack, H. J., & Schlanger, S. O. (1990). Stratigraphy, geochemistry and paleoceanography of organic-carbon rich Cretaceous sequences. In R. N. Ginsburg, & B. Beaudoin (Eds.), *Cretaceous resources, events and rhythms* (pp. 75–119). Dordrecht, Netherlands: Kluwer Academic Press.
- Berner, R. A. (2004). *The Phanerozoic carbon cycle:  $\text{CO}_2$  and  $\text{O}_2$*  (p. 158). Oxford, UK: Oxford University Press.
- Blakey, R. (2005). *Global paleogeography*. Retrieved from <http://jan.ucc.nau.edu/~rcb7/globaltext2.html>
- Blättler, C. L., Jenkyns, H. C., Reynard, L. M., & Henderson, G. M. (2011). Significant increases in global weathering during Oceanic Anoxic Events 1a and 2 indicated by calcium isotopes. *Earth and Planetary Science Letters*, 309, 77–88. <https://doi.org/10.1016/j.epsl.2011.06.029>
- Bottini, C., Cohen, A. S., Erba, E., Jenkyns, H. C., & Coe, A. L. (2012). Osmium isotope evidence for volcanism, weathering and ocean mixing during the early Aptian OAE 1a. *Geology*, 40, 583–586. <https://doi.org/10.1130/G33140.1>
- Bottini, C., & Erba, E. (2018). Mid-Cretaceous paleoenvironmental changes in the western Tethys. *Climate of the Past*, 14, 1147–1163. <https://doi.org/10.5194/cp-14-1147-2018>
- Bottini, C., Erba, E., Tiraboschi, D., Jenkyns, H. C., Schouten, S., & Sinninghe Damsté, J. S. (2015). Climate variability and ocean fertility during the Aptian stage. *Climate of the Past*, 11(3), 383–402. <https://doi.org/10.5194/cp-11-383-2015>
- Bottini, C., & Mutterlose, J. (2012). Integrated stratigraphy of Early Aptian black shales in the Boreal Realm: Calcareous nannofossil and stable isotope evidence for global and regional processes. *Newsletters on Stratigraphy*, 45, 115–137.
- Bown, P. R. (2005). Early to mid-Cretaceous calcareous nannoplankton from the Northwest Pacific Ocean, Leg 198, Shatsky Rise. *Proceedings of the Ocean Drilling Project Scientific Results*, 108, 1–82.
- Bown, P. R., Rutledge, D. C., Crux, J. A., & Gallagher, L. T. (1998). Lower Cretaceous. In P. R. Bown (Ed.), *Calcareous nannofossil biostratigraphy* (pp. 16–28). London: Micropalaeontological Society Publication Series Chapman and Hall.
- Bown, P. R., & Young, J. R. (1998). Techniques. In P. R. Bown (Ed.), *Calcareous nannofossil biostratigraphy*. London: Micropalaeontological Society Publication Series Chapman and Hall.
- Bralower, T. J., CoBabe, E., Clement, B., Sliter, W. V., Osburn, C. L., & Longoria, J. F. (1999). The record of global change in mid-Cretaceous (Barremian–Albian) sections from the Sierra Madre, northeastern Mexico. *Journal of Foraminiferal Research*, 29, 418–437.
- Bralower, T. J., Fullagar, P. D., Paull, C. K., Dwyer, G. S., & Leckie, R. M. (1997). Mid-Cretaceous strontium-isotope stratigraphy of deep-sea sections. *The Geological Society of America Bulletin*, 109, 1421–1442.
- Bralower, T. J., Leckie, R. M., Sliter, W. V., & Thierstein, H. R. (1995). An integrated Cretaceous microfossil biostratigraphy. In W. A. Berggren, D. V. Kent, M.-P. Aubry, & J. Hardenbol (Eds.), *Geochronology, time scales and global stratigraphic correlation* (Vol. 54, pp. 65–79). Tulsa, OK: The Society of Economic Paleontologists and Mineralogists special Publications (SEPM).
- Brehéret, J. (1988). Épisodes de sédimentation riche en matière organique dans les marnes bleues d'âge aptien et albien de la partie pélagique du bassin vocontien. *Bulletin de la Société Géologique de France*, 8, 349–356.
- Castro, J. M. (1998). *Las plataformas del Valanginiense superior-Albiense superior en el Prebético de Alicante* (PhD thesis). Granada: Universidad de Granada. Retrieved from <https://www.educacion.gob.es/teseo/mostrarRef.do?ref=176076>
- Castro, J. M., Company, M., de Gea, G. A., & Aguado, R. (2001). Biostratigraphy of the Aptian–Middle Cenomanian platform to basin domain in the Prebetic Zone of Alicante, SE Spain: Calibration between shallow water benthic and pelagic scales. *Cretaceous Research*, 22, 145–156. <https://doi.org/10.1006/cres.2000.0249>
- Castro, J. M., de Gea, G. A., Quijano, M. L., Aguado, R., Froehner, S., Naafs, B. D. A., & Pancost, R. D. (2019). Complex and protracted environmental and ecological perturbations during OAE 1a—Evidence from an expanded pelagic section from south Spain (western Tethys). *Global and Planetary Change*, 183, 103030. <https://doi.org/10.1016/j.gloplacha.2019.103030>
- Castro, J. M., de Gea, G. A., Ruiz-Ortiz, P. A., & Nieto, L. M. (2008). Development of carbonate platforms on an extensional (rifted) margin. The Valanginian–Albian record of the Prebetic of Alicante (SE Spain). *Cretaceous Research*, 29, 848–860. <https://doi.org/10.1016/j.cretres.2008.05.012>
- Castro, J. M., Jiménez de Cisneros, C., de Gea, G. A., Ruiz-Ortiz, P. A., Quijano, M. L., Caballero, E., & Pancost, R. D. (2014). La Formación Almadich en la Sierra de Mariola: Caracterización litológica, bioestratigráfica, geoquímica y mineralógica (Aptiense inferior, Cordillera Bética, Alicante). *Revista de la Sociedad Geológica de España*, 27, 27–136.
- Channell, J. E. T., Erba, E., Nakanishi, M., & Tamaki, K. (1995). Late Jurassic–Early Cretaceous timescales and oceanic magnetic anomaly block models. In W. A. Berggren, D. W. Kent, M. Aubry, & J. Hardenbol (Eds.), *Geochronology time scales and global stratigraphic correlation* (Vol. 54, pp. 51–63). Tulsa, OK: SEPM Special Publication.

- Chumakov, N. M., Zharkov, M. A., Herman, A. B., Doludenko, M. P., Kalandadze, N. N., Lebedev, E. L., et al. (1995). Climatic belts of the mid-Cretaceous time. *Stratigraphy and Geological Correlation*, 3, 241–260.
- Coccioni, A., Nesci, O., Tramontana, M., Wezel, F. C., & Moretti, E. (1987). Descrizione di un livello-guida “Radiolaritico-bituminoso ittiolitico” alla base delle marne a fucoidi nell’Appennino umbro-marchigiano. *Bollettino della Societa Geologica Italiana*, 106, 183–192.
- Coccioni, R. (2020). Revised upper Barremian–upper Aptian planktonic foraminiferal biostratigraphy of the Gorgo a Cerbara section (central Italy). *Newsletters on Stratigraphy*, 53/3, 275–295.
- Coccioni, R., Erba, E., & Premoli Silva, I. (1992). Barremian–Aptian calcareous plankton biostratigraphy from the Gorgo a Cerbara section (Marche, Central Italy) and implication for planktonic evolution. *Cretaceous Research*, 13, 517–537. [https://doi.org/10.1016/0195-6671\(92\)90015-1](https://doi.org/10.1016/0195-6671(92)90015-1)
- Coccioni, R., Luciani, V., & Marsili, A. (2006). Cretaceous Oceanic Anoxic Events and radially elongated chambered planktonic foraminifera: Paleocological and paleoceanographic implications. *Palaeogeography, Palaeoclimatology, Palaeoecology*, 235, 66–92. <https://doi.org/10.1016/j.palaeo.2005.09.024>
- Cramer, B. S., & Jarvis, I. (2020). Carbon isotope stratigraphy. In F. M. Gradstein, J. G. Ogg, M. D. Schmitz, & G. M. Ogg (Eds.), *The geologic time scale 2020*. Amsterdam: Elsevier. <https://doi.org/10.1016/B978-0-12-824360-2.00011-5>
- Davies, A., Gréselle, B., Hunter, S. J., Baines, A., Robson, C., Haywood, A. M., et al. (2020). Assessing the impact of aquifer-eustasy on short-term Cretaceous sea-level. *Cretaceous Research*, 112, 104445. <https://doi.org/10.1016/j.cretres.2020.104445>
- de Gea, G. A., Aguado, R., Castro, J. M., Molina, J. M., O’Dogherty, L., & Ruiz Ortiz, P. A. (2008). Lower Aptian Subbetic organic-rich facies, radiolarites and associated deposits: The local expression of Oceanic Anoxic Event 1a (Carbonero Formation, southern Spain). *Cretaceous Research*, 29, 861–870. <https://doi.org/10.1016/j.cretres.2008.05.011>
- de Gea, G. A., Castro, J. M., Aguado, R., Ruiz Ortiz, P. A., & Company, M. (2003). Lower Aptian carbon-isotope stratigraphy from a distal carbonate shelf setting: The Cau section, Prebetic Zone, SE Spain. *Palaeogeography, Palaeoclimatology, Palaeoecology*, 200, 207–219. [https://doi.org/10.1016/S0031-0182\(03\)00451-6](https://doi.org/10.1016/S0031-0182(03)00451-6)
- Dercourt, J., Gaetani, M., Vrielynck, B., Barrier, E., Biju-Duval, B., Brunet, M. F., et al. (Eds.). (2000). *Atlas Peri-Tethys paleogeographical maps*, Paris, France: CCGM/CGMW.
- Dumitrescu, M., & Brassell, S. C. (2005). Biogeochemical assessment of sources of organic matter and paleoproductivity during the Early Aptian Oceanic Anoxic Event at Shatsky Rise, ODP Leg 198. *Organic Geochemistry*, 36, 1002–1022. <https://doi.org/10.1016/j.orggeochem.2005.03.001>
- Dumitrescu, M., Brassell, S. C., Schouten, S., Hopmans, E. C., & Sinninghe-Damste, J. S. (2006). Instability in tropical Pacific sea-surface temperatures during the early Aptian. *Geology*, 34, 833–836. <https://doi.org/10.1130/G22882.1>
- Dummann, W., Steinig, S., Hofmann, P., Flögel, S., Osborne, A. H., Frank, M., et al. (2020). The impact of Early Cretaceous gateway evolution on ocean circulation and organic carbon burial in the emerging South Atlantic and Southern Ocean basins. *Earth and Planetary Science Letters*, 530, 115890. <https://doi.org/10.1016/j.epsl.2019.115890>
- Dunham, R. J. (1962). Classification of carbonate rocks according to depositional texture. In W. E. Ham (Ed.), *Classification of carbonate rocks* (Vol. 1, pp. 108–121). American Association of Petroleum Geologists Memoir.
- Erba, E. (1994). Nannofossils and superplumes: The early Aptian ‘nannoconid crisis’. *Paleoceanography*, 9, 483–501. <https://doi.org/10.1029/94PA00258>
- Erba, E. (1996). The Aptian stage. In P. F. Rawson, A. V. Dhondt, J. M. Hancock, & W. J. Kennedy (Eds.), *Proceedings of the 2nd International Symposium on Cretaceous Stage Boundaries* (Vol. 66, pp. 31–43). Bulletin de l’Institut Royal des Sciences Naturelles de Belgique.
- Erba, E. (2004). Calcareous nannofossils and Mesozoic Oceanic Anoxic Events. *Marine Micropaleontology*, 52, 85–106.
- Erba, E., Bottini, C., Weissert, J. H., & Keller, C. E. (2010). Calcareous nannoplankton response to surface-water acidification around Oceanic Anoxic Event 1a. *Science*, 329, 428–432. <https://doi.org/10.1126/science.1188886>
- Erba, E., Channell, J. E. T., Claps, M., Jones, C., Larson, R. L., Opdyke, B., et al. (1999). Integrated stratigraphy of the Cismon Apticore (Southern Alps, Italy): A “reference section” for the Barremian–Aptian interval at low latitudes. *Journal of Foraminiferal Research*, 29, 371–391.
- Erba, E., Duncan, R. A., Bottini, C., Tiraboschi, D., Weissert, H., Jenkyns, H. C., & Malinverno, A. (2015). Environmental consequences of Ontong-Java Plateau and Kerguelen Plateau volcanism. In C. R. Neal, W. W. Sager, T. Sano, & E. Erba (Eds.), *The origin, evolution, and environmental impact of oceanic large igneous provinces* (Vol. 511, pp. 271–303). Geological Society of America Special Paper. [https://doi.org/10.1130/2015.2511\(15\)](https://doi.org/10.1130/2015.2511(15))
- Erbacher, J., & Thurow, J. (1997). Influence of Oceanic Anoxic Events on the evolution of mid-Cretaceous radiolaria in the North Atlantic and western Tethys. *Marine Micropaleontology*, 30, 139–158.
- Fernandez-Mendiola, P. A., Mendicoa, J., Owen, H. G., & Garcia-Mondéjar, J. (2018). The Early Aptian (Cretaceous) stratigraphy of Mount Pagasarri (N Spain): Oceanic Anoxic Event-1a. *Geological Journal*, 53, 1802–1822. <https://doi.org/10.1002/gj.3008>
- Föllmi, K. B. (2012). Early Cretaceous life, climate and anoxia. *Cretaceous Research*, 35, 230–257. <https://doi.org/10.1016/j.cretres.2011.12.005>
- Föllmi, K. B., Godet, A., Bodin, S., & Linder, P. (2006). Interactions between environmental change and shallow water carbonate buildup along the northern Tethyan margin and their impact on the Early Cretaceous carbon isotope record. *Paleoceanography*, 21, PA4211. <https://doi.org/10.1029/2006PA001313>
- Föllmi, K. B., Weissert, H., Bisping, M., & Funk, H. (1994). Phosphogenesis, carbon isotope stratigraphy, and carbonate-platform evolution along the Lower Cretaceous northern Tethyan margin. *The Geological Society of America Bulletin*, 106, 729–746.
- Frey, E. A., Coffin, M. F., Wallace, P. J., & Weis, D. (2003). Leg 183 synthesis: Kerguelen Plateau–Broken Ridge—A large igneous province. In F. A. Frey, M. F. Coffin, P. J. Wallace, & P. G. Quilty (Eds.), *Proceedings of the Ocean Drilling Program, Scientific Results* (Vol. 183, pp. 1–48). College Station, TX: Ocean Drilling Program. Retrieved from [http://www-odp.tamu.edu/publications/183\\_SR/VOLUME/SYNTH/SYNTH.PDF](http://www-odp.tamu.edu/publications/183_SR/VOLUME/SYNTH/SYNTH.PDF)
- Friedrich, O., Reichelt, K., Herrle, J. O., Lehmann, J., Pross, J., & Hemleben, C. (2003). Formation of the Late Aptian Niveau Fallot black shales in the Vocontian Basin (SE France): Evidence from foraminifera, palynomorphs, and stable isotopes. *Marine Micropaleontology*, 49, 65–85.
- Gibbs, S. J., Robinson, S. A., Bown, P. R., Jones, T. D., & Henderiks, J. (2011). Comment on ‘Calcareous nannoplankton response to surface-water acidification around Oceanic Anoxic Event 1a’. *Science*, 332, 175.
- Giorgioni, M., Keller, C. E., Weissert, H., Hochuli, P. A., & Bernasconi, S. M. (2015). Black shales – from coolhouse to greenhouse (early Aptian). *Cretaceous Research*, 56, 716–731. <http://dx.doi.org/10.1016/j.cretres.2014.12.003>
- Giraud, F., Pittet, B., Grosheny, D., Baudin, F., Lécuyer, C., & Sakamoto, T. (2018). The paleoceanographic crisis of the Early Aptian (OAE 1a) in the Vocontian Basin (SE France). *Palaeogeography, Palaeoclimatology, Palaeoecology*, 511, 483–505. <https://doi.org/10.1016/j.palaeo.2018.09.014>

- Gradstein, F. M., Ogg, J. G., Schmitz, M. D., & Ogg, G. M. (Eds.). (2020). *The geologic time scale 2020*. Amsterdam: Elsevier. <https://doi.org/10.1016/C2020-1-02369-3>
- Graziano, R. (2013). Sedimentology, biostratigraphy and event stratigraphy of the Early Aptian Oceanic Anoxic Event (OAE1a) in the Apulia Carbonate Platform Margin-Ionian Basin System (Gargano Promontory, southern Italy). *Cretaceous Research*, 39, 78–111. <http://dx.doi.org/10.1016/j.cretres.2012.05.014>
- Haq, B. U. (2014). Cretaceous eustasy revisited. *Global and Planetary Change*, 113, 44–58. <http://dx.doi.org/10.1016/j.gloplacha.2013.12.007>
- Hay, W. W. (2017). Toward understanding Cretaceous climate—An updated review. *Science China Earth Sciences*, 60, 5–19. <https://doi.org/10.1007/s11430-016-0095-9>
- Heimhofer, U., Hochuli, P. A., Herrle, J. O., Andersen, N., & Weissert, H. (2004). Absence of major vegetation and palaeoatmospheric pCO<sub>2</sub> changes associated with Oceanic Anoxic Event 1a (Early Aptian, SE France). *Earth and Planetary Science Letters*, 223, 303–318.
- Herrle, J. O., Köbler, P., & Bollmann, J. (2010). Paleoceanographic differences of early Late Aptian black shale events in the Vocontian Basin (SE France). *Palaeogeography, Palaeoclimatology, Palaeoecology*, 297, 367–376. <https://doi.org/10.1016/j.palaeo.2010.08.015>
- Herrle, J. O., Köbler, P., Friedrich, O., Erlenkeuser, H., & Hemleben, C. (2004). High-resolution carbon isotope records of the Aptian to Lower Albian from SE France and the Mazagan Plateau (DSDP site 545): A stratigraphic tool for paleoceanographic and paleobiologic reconstruction. *Earth and Planetary Science Letters*, 218, 149–161. [https://doi.org/10.1016/S0012-821X\(03\)00646-0](https://doi.org/10.1016/S0012-821X(03)00646-0)
- Herrle, J. O., & Mutterlose, J. (2003). Calcareous nannofossils from the Aptian–Lower Albian of southeast France: Palaeoecological and biostratigraphic implications. *Cretaceous Research*, 24, 1–22. [https://doi.org/10.1016/S0195-6671\(03\)00023-5](https://doi.org/10.1016/S0195-6671(03)00023-5)
- Hochuli, P. A., Menegatti, A. P., Weissert, H., Riva, A., Erba, E., & Premoli Silva, I. (1999). Episodes of high productivity and cooling in the early Aptian Alpine Tethys. *Geology*, 27, 657–660.
- Huber, B. T., & Leckie, R. M. (2011). Planktic foraminiferal species turnover across deep-sea Aptian/Albian boundary sections. *Journal of Foraminiferal Research*, 41, 53–95.
- Huber, B. T., Petrizzo, M. R., Young, J. R., Falzoni, F., Gilardoni, S. E., Bown, P. R., & Wade, B. S. (2016). Pforams@microtax: A new online taxonomic database for planktonic foraminifera. *Micropaleontology*, 62, 429–438.
- Huck, S., Heimhofer, U., & Immenhauser, A. (2012). Early Aptian algal bloom in a neritic proto-North Atlantic setting: Harbinger of global change related to OAE1a? *GSA Bulletin*, 124, 1810–1825.
- Huck, S., Heimhofer, U., Immenhauser, A., & Weissert, H. (2013). Carbon-isotope stratigraphy of Early Cretaceous (Urgonian) shoal-water deposits: Diachronous changes in carbonate-platform production in the north-western Tethys. *Sedimentary Geology*, 290, 157–174. <http://dx.doi.org/10.1016/j.sedgeo.2013.03.016>
- Huck, S., Heimhofer, U., Rameil, N., Bodin, S., & Immenhauser, A. (2011). Strontium and carbon-isotope chronostratigraphy of Barremian–Aptian shoal-water carbonates: Northern Tethyan platform drowning predates OAE 1a. *Earth and Planetary Science Letters*, 304, 547–558.
- Huck, S., Rameil, N., Korbar, T., Heimhofer, U., Wiczorek, T. D., & Immenhauser, A. (2010). Latitudinally different responses of Tethyan shoal-water carbonate systems to the Early Aptian Oceanic Anoxic Event (OAE 1a). *Sedimentology*, 57, 1585–1614.
- Hu, X., Li, J., Hanz, Z., & Li, Y. (2020). Two types of hyperthermal events in the Mesozoic–Cenozoic: Environmental impacts, biotic effects, and driving mechanisms. *Science China Earth Sciences*, 63, 1041–1058.
- Hu, X., Zhao, K., Yilmaz, I. O., & Li, Y. (2012). Stratigraphic transition and palaeoenvironmental changes from the Aptian Oceanic Anoxic Event 1a (OAE1a) to the oceanic red bed 1 (ORB1) in the Yenicesihlar section, central Turkey. *Cretaceous Research*, 38, 40–51.
- Immenhauser, A. (2005). High-rate sea-level change during the Mesozoic: New approaches to an old problem. *Sedimentary Geology*, 175, 277–296. <https://doi.org/10.1016/j.sedgeo.2004.12.016>
- Immenhauser, A., Hillgärtner, H., & van Bentum, E. (2005). Microbial-foraminiferal episodes in the Early Aptian of the southern Tethyan margin: Ecological significance and possible relation to Oceanic Anoxic Event 1a. *Sedimentology*, 52, 77–99.
- Immenhauser, A., Schlager, W., Burns, S. J., Scott, R. W., Geel, T., Lehmann, J., et al. (1999). Late Aptian to Late Albian sea-level fluctuations constrained by geochemical and biological evidence (Nahr Umr Fm Oman). *Journal of Sedimentary Research*, 69, 434–446.
- Jahren, A. H., Arens, N. C., Sarmiento, G., Guerrero, J., ... Amundson, R. (2001). Terrestrial record of methane hydrate dissociation in the Early Cretaceous. *Geology*, 29(2), 159. [http://doi.org/10.1130/0091-7613\(2001\)029<0159:tromhd>2.0.co;2](http://doi.org/10.1130/0091-7613(2001)029<0159:tromhd>2.0.co;2)
- Jahren, A. H., Conrad, C. P., Crystal Arens, N., Mora, G., & Lithgow-Bertelloni, C. (2005). A plate tectonic mechanism for methane hydrate release along subduction zones. *Earth and Planetary Science Letters*, 236, 691–704.
- Jarvis, I., Lignum, J. S., Gröcke, D. R., Jenkyns, H. C., & Pearce, M. A. (2011). Black shale deposition, atmospheric CO<sub>2</sub> drawdown, and cooling during the Cenomanian–Turonian Oceanic Anoxic Event. *Paleoceanography*, 26, PA3201. <https://doi.org/10.1029/2010PA002081>
- Jarvis, I., Trabucho-Alexandre, J., Gröcke, D. R., Uličný, D., & Laurin, J. (2015). Intercontinental correlation of organic carbon and carbonate stable isotope records: Evidence of climate and sea-level change during the Turonian (Cretaceous). *The Depositional Record*, 1, 53–90. <https://doi.org/10.1002/dep2.6>
- Jenkyns, H. C. (1995). Carbon-isotope stratigraphy and paleoceanographic significance of the Lower Cretaceous shallow-water carbonates of Resolution Guyot, Mid-Pacific Mountains. In E. L. Winterer, W. W. Sager, J. V. Firth, & J. M. Sinton (Eds.), *Proceedings of the Ocean Drilling Program, Scientific Results* (Vol. 143, pp. 99–104). College Station, TX: Ocean Drilling Program.
- Jenkyns, H. C. (2010). Geochemistry of Oceanic Anoxic Events. *Geochemistry, Geophysics, Geosystems*, 11, Q03004. <https://doi.org/10.1029/2009GC002788>
- Jenkyns, H. C. (2018). Transient cooling episodes during Cretaceous Oceanic Anoxic Events with special reference to OAE 1a (Early Aptian). *Philosophical Transactions of the Royal Society A*, 376, 20170073. <http://dx.doi.org/10.1098/rsta.2017.0073>
- Jones, C. E., & Jenkyns, H. C. (2001). Seawater strontium isotopes, Oceanic Anoxic Events, and seafloor hydrothermal activity in the Jurassic and Cretaceous. *American Journal of Science*, 301, 112–149. <https://doi.org/10.2475/ajs.301.2.112>
- Kemp, D. B., Coe, A., Cohen, A., & Schwark, L. (2005). Astronomical pacing of methane release in the Early Jurassic period. *Nature*. <https://doi.org/10.1038/nature04037>
- Kennedy, W. J., Gale, A. S., Bown, P. R., Caron, M., Davey, R. J., Gröcke, D. R., & Wray, D. S. (2000). Integrated stratigraphy across the Aptian–Albian boundary in the Marnes Bleues, at the Col de Pré-Guittard, Arnayon (Drôme), and at Tartonne (Alpes-de-Haute-Provence), France: A candidate global boundary stratotype section and boundary point for the base of the Albian Stage. *Cretaceous Research*, 21, 591–720. <https://doi.org/10.1006/crel.2000.0223>
- Kuhnt, W., Holbourn, A., & Moullade, M. (2011). Transient global cooling at the onset of early Aptian Oceanic Anoxic Event (OAE) 1a. *Geology*, 39, 323–326. <https://doi.org/10.1130/G31554.1>
- Kump, L. R., & Arthur, M. A. (1999). Interpreting carbon-isotope excursions: Carbonates and organic matter. *Chemical Geology*, 161, 18–198.

- Larson, R. L., & Erba, E. (1999). Onset of the mid-Cretaceous greenhouse in the Barremian–Aptian: Igneous events and the biological, sedimentary and geochemical responses. *Paleoceanography*, *14*, 663–678. <https://doi.org/10.1029/1999PA000040>
- Lechler, M., Pogge von Strandmann, P. A. P., Jenkyns, H. C., Prosser, G., & Parente, M. (2015). Lithium-isotope evidence for enhanced silicate weathering during OAE 1a (Early Aptian Selli event). *Earth and Planetary Science Letters*, *432*, 210–222. <https://doi.org/10.1016/j.epsl.2015.09.052>
- Leckie, R. M., Bralower, T. J., & Cashman, R. (2002). Oceanic Anoxic Events and plankton evolution: Biotic response to tectonic forcing during the Mid-Cretaceous. *Paleoceanography*, *17*, PA1041. <https://doi.org/10.1029/2001PA000623>
- Li, Y., Bralower, T. J., Montañez, I. P., Osleger, D. A., Arthur, M. A., Bice, D. M., et al. (2008). Toward an orbital chronology for the early Aptian Oceanic Anoxic Event (OAE1a, ~120 Ma). *Earth and Planetary Science Letters*, *271*, 88–100. <https://doi.org/10.1016/j.epsl.2008.03.055>
- Lorenzen, J., Kuhnt, W., Holbourn, A., Flögel, S., Moullade, M., & Tronchetti, G. (2013). A new sediment core from the Bedoulian (Lower Aptian) stratotype at Roquefort–La Bédoule, SE France. *Cretaceous Research*, *39*, 6–16. <https://doi.org/10.1016/j.cretres.2012.03.019>
- Loutit, T. S., & Kennett, J. P. (1979). Application of carbon isotope stratigraphy to late Miocene shallow marine sediments, New Zealand. *Science*, *15*, 1196–1199. <https://doi.org/10.1126/science.204.4398.1196>
- Ludvigson, G. A., Joeckel, R. M., Murphy, L. R., Stockli, D. F., González, L. A., Suarez, C. A., et al. (2015). The emerging terrestrial record of Aptian–Albian global change. *Cretaceous Research*, *56*, 1–24. <https://doi.org/10.1016/j.cretres.2014.11.008>
- Malinverno, A., Erba, E., & Herbert, T. D. (2010). Orbital tuning as an inverse problem: Chronology of the early Aptian Oceanic Anoxic Event 1a (Selli Level) in the Cismon APTICORE. *Paleoceanography*, *25*, PA2203. <https://doi.org/10.1029/2009PA001769>
- Malinverno, A., Hildebrandt, J., Tominaga, M., & Channell, J. E. T. (2012). M-sequence geomagnetic polarity time scale (MHTC12) that steadies global spreading rates and incorporates astrochronology constraints. *Journal of Geophysical Research*, *117*, B06104. <https://doi.org/10.1029/2012JB009260>
- Martin-Chivelet, J., Berasategui, X., Rosales, I., Vilas, L., Vera, J. A., Caus, E., et al. (2002). Cretaceous. In W. Gibbons, & T. Moreno (Eds.), *The geology of Spain*. London: The Geological Society.
- Martin-Chivelet, J., López-Gómez, J., Aguado, R., Arias, C., Arribas, J., Arribas, M. E., et al. (2019). The Late Jurassic–Early Cretaceous Rifting. In C. Quesada, & J. T. Oliveira (Eds.), *The geology of Iberia: A geodynamic approach. Regional geology reviews*. Cham: Springer. [https://doi.org/10.1007/978-3-030-11295-0\\_5](https://doi.org/10.1007/978-3-030-11295-0_5)
- Martinez, M., Aguado, R., Company, M., Sandoval, J., & O’Doherty, L. (2020). Integrated astrochronology of the Barremian Stage (Early Cretaceous) and its biostratigraphic subdivisions. *Global and Planetary Change*, *195*, 1–24. <https://doi.org/10.1016/j.gloplacha.2020.103368>
- Masse, J. P., Bellion, Y., Benkheilil, J., Boulin, J., Corneé, J. J., Dercourt, J., et al. (1993). Lower Aptian palaeoenvironments 114–112 Ma. In J. Dercourt, L. E. Ricou, & B. Vrielynck (Eds.), *Atlas Tethys palaeoenvironmental maps*. Rueil-Malmaison: BEICIP-FRANLAB.
- Masse, J. P., Bouaziz, S., Amon, E. O., Baraboshkin, E., Tarkowski, R., Bergerat, F., et al. (2000). Early Aptian (94.7–93.5 Ma). In J. Dercourt, M. Gaetani, B. Vrielynck, E. Barrier, B. Biju-Duval, M. F. Brunet, et al. (Eds.), *Peri-tethys Palaeogeographical Atlas*. Paris, France: CCGM/CGMW.
- Masse, J.-P., & Fenerci-Masse, M. (2011). Drowning discontinuities and stratigraphic correlation in platform carbonates. The late Barremian–early Aptian record of southeast France. *Cretaceous Research*, *32*, 659–684.
- Masse, J.-P., & Fenerci-Masse, M. (2013). Drowning events, development and demise of carbonate platforms and controlling factors: The Late Barremian–Early Aptian record of Southeast France. *Sedimentary Geology*, *298*, 28–52.
- Maurer, F., van Buchem, F. S. P., Eberli, G. P., Pierson, B. J., Raven, M. J., Larsen, P., et al. (2013). Late Aptian long-lived glacio-eustatic lowstand recorded on the Arabian Plate. *Terra Nova*, *25*, 87–94.
- McAnena, A., Flögel, S., Hofmann, P., Herrle, J. O., Griesand, A., Pross, J., et al. (2013). Atlantic cooling associated with a marine biotic crisis during the mid-Cretaceous period. *Nature Geoscience*, *6*, 558–561. <https://doi.org/10.1038/ngeo1850>
- Méhay, S., Keller, C. E., Bernasconi, S. M., Weissert, H., Erba, E., Bottini, C., & Hochuli, P. A. (2009). A volcanic CO<sub>2</sub> pulse triggered the Cretaceous Oceanic Anoxic Event 1a and a biocalcification crisis. *Geology*, *37*, 819–822. <https://doi.org/10.1130/G30100A.1>
- Melinte, M., & Mutterlose, J. (2001). A Valanginian (Early Cretaceous) ‘boreal nannoplankton excursion’ in sections from Romania. *Marine Micropaleontology*, *43*, 1–25.
- Menegatti, A. P., Weissert, H., Brown, R. S., Tyson, R. V., Farrimond, P., Strasser, A., & Caron, M. (1998). High-resolution  $\delta^{13}\text{C}$  stratigraphy through the early Aptian “Livello Selli” of the Alpine Tethys. *Paleoceanography*, *13*, 530–545. <https://doi.org/10.1029/98PA01793>
- Millán, M. I., Weissert, H. J., Fernández-Mendiola, P. A., & García-Mondéjar, J. (2009). Impact of Early Aptian carbon cycle perturbations on evolution of a marine shelf system in the Basque-Cantabrian Basin (Aralar, N Spain). *Earth and Planetary Science Letters*, *287*, 392–401.
- Millán, M. I., Weissert, H. J., & López-Horgue, M. A. (2014). Expression of the late Aptian cold snaps and the OAE1b in a highly subsiding carbonate platform (Aralar, northern Spain). *Palaeogeography, Palaeoclimatology, Palaeoecology*, *411*, 167–179. <https://doi.org/10.1016/j.palaeo.2014.06.024>
- Misumi, K., & Yamanaka, Y. (2008). Ocean anoxic events in the mid-Cretaceous simulated by a 3-D biogeochemical general circulation model. *Cretaceous Research*, *29*, 893–900.
- Moreno-Bedmar, J. A., Company, M., Sandoval, J., Tavera, J. M., Bover-Arnal, T., Salas, R., et al. (2012). Lower Aptian ammonite and carbon isotope stratigraphy in the eastern Prebetic Domain (Betic Cordillera, southeastern Spain). *Geológica Acta*, *10*, 333–350. <https://doi.org/10.1344/105.000001752>
- Moullade, M., Bellier, J. P., & Tronchetti, G. (2002). Hierarchy of criteria, evolutionary processes and taxonomic simplification in the classification of Lower Cretaceous planktonic foraminifera. *Cretaceous Research*, *23*, 111–148. <https://doi.org/10.1006/cres.2002.0304>
- Moullade, M., Tronchetti, G., Granier, B., Bornemann, A., Kuhnt, W., & Lorenzen, J. (2015). High-resolution integrated stratigraphy of the OAE1a and enclosing strata from core drillings in the Bedoulian stratotype (Roquefort–La Bédoule, SE France). *Cretaceous Research*, *56*, 119–140. <https://doi.org/10.1016/j.cretres.2015.03.004>
- Mutterlose, J., & Böckel, B. (1998). The Barremian–Aptian interval in NW Germany: A review. *Cretaceous Research*, *19*, 539–568. <https://doi.org/10.1006/cres.1998.0119>
- Mutterlose, J., & Bottini, C. (2013). Early Cretaceous chalks from the North Sea giving evidence for global change. *Nature Communications*, *4*, 1686. <https://doi.org/10.1038/ncomms2698>
- Mutterlose, J., Bottini, C., Schouten, S., & Sinninghe-Damsté, J. S. (2014). High sea-surface temperatures during the early Aptian Oceanic Anoxic Event 1a in the Boreal Realm. *Geology*, *42*, 439–442. <https://doi.org/10.1130/G35394.1>
- Mutterlose, J., Pauly, S., & Steuber, T. (2009). Temperature controlled deposition of early Cretaceous (Barremian–early Aptian) black shales in an epicontinental sea. *Palaeogeography, Palaeoclimatology, Palaeoecology*, *273*, 330–345. <https://doi.org/10.1016/j.palaeo.2008.04.026>

- Naafs, B. D. A., Castro, J. A., de Gea, G. A., Quijano, M. L., Schmidt, D. N., & Pancost, R. D. (2016). Gradual and sustained carbon dioxide release during Aptian Oceanic Anoxic Event 1a. *Nature Geoscience*, 9, 135–139. <https://doi.org/10.1038/ngeo2627>
- Naafs, B. D. A., & Pancost, R. D. (2016). Sea-surface temperature evolution across Aptian Oceanic Anoxic Event 1a. *Geology*, 44, 959–962. <https://doi.org/10.1130/G38575.1>
- Najarro, M., Rosales, I., & Martín-Chivelet, J. (2011). Major palaeoenvironmental perturbation in an Early Aptian carbonate platform: Prelude of the Oceanic Anoxic Event 1a? *Sedimentary Geology*, 235, 50–71.
- Nelson, D. W., & Sommers, L. E. (1996). Total carbon, organic carbon, and organic matter: Methods of soil analysis Part 3. *Chemical Methods*, 5, 961–1010.
- O'Brien, C. L., Robinson, S. A., Pancost, R. D., Damsté, J. S. S., Schouten, S., Lunt, D. J., et al. (2017). Cretaceous sea-surface temperature evolution: Constraints from TEX86 and planktonic foraminiferal oxygen isotopes. *Earth-Science Reviews*, 172, 224–247.
- Ogg, J. G., Ogg, G. M., & Gradstein, F. M. (2016). 13-Cretaceous. In J. G. Ogg, G. M. Ogg, & F. M. Gradstein (Eds.), *A concise geologic time scale*. Amsterdam: Elsevier.
- Olierook, H. J. H., Jourdan, F., & Merle, R. E. (2019). Age of the Barremian–Aptian boundary and onset of the Cretaceous Normal Superchron. *Earth-Science Reviews*, 197, 102906. <https://doi.org/10.1016/j.earscirev.2019.102906>
- Olivet, J. M. (1996). La cinématique de la plaque ibérique. *Bulletin des Centres Recherche Exploration et Production Elf-Aquitaine*, 20, 131–195.
- Perch-Nielsen, K. (1985). Mesozoic calcareous nannofossils. In H. M. Bolli, J. B. Saunders, & K. Perch-Nielsen (Eds.), *Plankton stratigraphy*. Cambridge, London, New York, NY, New Rochelle, Melbourne, Sydney: Cambridge University Press.
- Polteau, S., Hendriks, B. W. H., Planke, S., Ganer, M., Corfu, F., Faleide, J. I., et al. (2016). The Early Cretaceous Barents Sea Sill complex: Distribution, <sup>40</sup>Ar/<sup>39</sup>Ar geochronology, and implications for carbon gas formation. *Paleoogeography, Palaeoclimatology, Palaeoecology*, 441, 83–95. <https://doi.org/10.1016/j.palaeo.2015.07.007>
- Quijano, M. L., Castro, J. M., Pancost, R. D., de Gea, G. A., Najarro, M., Aguado, R., et al. (2012). Organic geochemistry, stable isotopes, and facies analysis of the Early Aptian OAE—New records from Spain (western Tethys). *Paleoogeography, Palaeoclimatology, Palaeoecology*, 365–366, 276–293. <https://doi.org/10.1016/j.palaeo.2012.09.033>
- Raschini, A. (2012). Shallow water carbonate platforms (Late Aptian–Early Albian, Southern Apennines) in the context of supraregional to global changes: Re-appraisal of palaeoecologic events as reflectors of carbonate factory response. *Solid Earth*, 3, 225–249. <http://dx.doi.org/10.5194/se-3-225-2012>
- Robinson, S. A., Williams, T., & Bown, P. R. (2004). Fluctuations in biosiliceous production and the generation of Early Cretaceous Oceanic Anoxic Events in the Pacific Ocean (Shatsky Rise, Ocean Drilling Program Leg 198). *Paleoceanography*, 19, PA4024. <https://doi.org/10.1029/2004PA001010>
- Ruiz-Ortiz, P. A. (1980). *Análisis de facies del Mesozoico de las Unidades Intermedias (Entre Castril, prov. de Granada y Jaén)* (PhD thesis). Granada: Universidad de Granada. Retrieved from <https://www.educacion.gob.es/teseo/mostratRef.do?ref=11076>
- Ruiz-Ortiz, P. A., & Castro, J. M. (1998). Carbonate depositional sequences in shallow to pelagic platform deposits. Aptian. Prebetic of Alicante (SE Spain). *Bulletin de la Societe Geologique de France*, 169, 21–33.
- Ruiz-Ortiz, P. A., Castro, J. M., de Gea, G. A., Jarvis, I., Molina, J. M., Nieto, L. M., et al. (2016). New drilling of the early Aptian OAE1a: The Cau core (Prebetic zone, south-eastern Spain). *Scientific Drilling*, 21, 41–46. <https://doi.org/10.5194/sd-21-41-2016>
- Sánchez-Hernández, Y., & Maurrasse, F. (2016). The influence of regional factors in the expression of Oceanic Anoxic Event 1a (OAE1a) in the semi-restricted Organyà Basin, south-central Pyrenees, Spain. *Paleoogeography, Palaeoclimatology, Palaeoecology*, 441, 582–598.
- Scott, R. W. (2016). Barremian–Aptian–Albian carbon isotope segments as chronostratigraphic signals: Numerical age calibration and durations. *Stratigraphy*, 13, 21–47.
- Scholle, P., & Arthur, M. A. (1980). Carbon isotopic fluctuations in pelagic limestones: Potential stratigraphic and petroleum exploration tool. *American Association of Petroleum Geologists Bulletin*, 64, 67–87. <https://doi.org/10.1306/2F91892D-16CE-11D7-8645000102C1865D>
- Skelton, P. W. (Ed.). (2003). *The Cretaceous world*. Cambridge, UK: Cambridge University Press and The Open University. Retrieved from <https://www.cambridge.org/tv/academic/subjects/earth-and-environmental-science/sedimentology-and-stratigraphy/cretaceous-world?format=HB#bookPeople>
- Skelton, P. W., Castro, J. M., & Ruiz-Ortiz, P. A. (2019). Aptian carbonate platform development in the Southern Iberian Palaeomargin (Prebetic of Alicante, SE Spain). *BSGF-Earth Sciences Bulletin*, 190, 3. <https://doi.org/10.1051/bsgf/2019001>
- Skelton, P. W., & Gili, E. (2012). Rudists and carbonate platforms in the Aptian: A case study on biotic interactions with ocean chemistry and climate. *Sedimentology*, 59, 81–117. <https://doi.org/10.1111/j.1365-3091.2011.01292.x>
- Stein, M., Follmi, K. B., Westermann, S., Godet, A., Adatte, T., Matera, V., et al. (2012). Progressive palaeoenvironmental change during the Late Barremian–Early Aptian as prelude to Oceanic Anoxic Event 1a: Evidence from the Gorgo a Cerbara section (Umbria–Marche basin, central Italy). *Paleoogeography, Palaeoclimatology, Palaeoecology*, 302, 396–406.
- Steinig, S., Dummann, W., Park, W., Latif, M., Kusch, S., Hofmann, & Flögel, S. (2020). Evidence for a regional warm bias in the Early Cretaceous TEX<sub>86</sub> record. *Earth and Planetary Science Letters*, 539, 116184.
- Tarduno, J. A., Lowrie, W., Sliter, W. V., Bralower, T. J., ... Heller, F. (1992). Reversed polarity characteristic magnetizations in the Albian Contessa Section, Umbrian Apennines, Italy: Implications for the existence of a Mid-Cretaceous mixed polarity interval. *Journal of Geophysical Research*, 97(B1), 241. <http://doi.org/10.1029/91jb02257>
- Tarduno, J. A., Sliter, W. V., Bralower, T. J., McWILLIAMS, M., Premoli-Silva, I., ... Ogg, J. G. (1989). M-sequence reversals recorded in DSDP sediment cores from the western Mid-Pacific Mountains and Magellan Rise. *Geological Society of America Bulletin*, 101(10), 1306–1316. [http://doi.org/10.1130/0016-7606\(1989\)101<1306:mssrid>2.3.co;2](http://doi.org/10.1130/0016-7606(1989)101<1306:mssrid>2.3.co;2)
- Tarduno, J. A., Sliter, W. V., Kroenke, L., Leckie, M., Mayer, H., Mahoney, J. J., et al. (1991). Rapid formation of Ontong Java Plateau by Aptian mantle plume volcanism. *Science*, 254(5030), 399–403. <https://doi.org/10.1126/science.254.5030.399>
- Tejada, M. L. G., Suzuki, K., Kuroda, J., Coccioni, R., Mahoney, J. J., Ohkouchi, N., & Tatsumi, Y. (2009). Ontong-Java Plateau eruption as a trigger for the early Aptian Oceanic Anoxic Event. *Geology*, 37, 855–858. <https://doi.org/10.1130/G25763A.1>
- Timm, C., Hoernle, K., Werner, R., Hauff, F., van den Bogaard, P., Michael, P., et al. (2011). Age and geochemistry of the oceanic Manihiki Plateau, SW Pacific: New evidence for a plume origin. *Earth and Planetary Science Letters*, 304, 135–146. <https://doi.org/10.1016/j.epsl.2011.01.025>
- Vahrenkamp, V. C. (2010). Chemostratigraphy of the Lower Cretaceous Shu'aiba Formation: A  $\delta^{13}\text{C}$  reference profile for the Aptian Stage from the southern Neo-Tethys Ocean. *GeoArabia Special Publication*, 4, 107–137.
- Van Breugel, Y., Schouten, S., Tsikos, H., Erba, E., Price, G. D., & Sinninghe Damsté, J. S. (2007). Synchronous negative carbon isotope shifts in marine and terrestrial biomarkers at the onset of the early Aptian Oceanic Anoxic Event 1a: Evidence for the release of  $^{13}\text{C}$ -depleted carbon into the atmosphere. *Paleoceanography*, 22, PA1210. <https://doi.org/10.1029/2006pa001341>

- Van Helmond, N. A. G. M., Sluijs, A., Reichert, G.-J., Sinninghe-Damsté, J. S., Slomp, C. P., & Brinkhuis (2013). A perturbed hydrological cycle during Oceanic Anoxic Event 2. *Geology*, *42*, 123–126. <https://doi.org/10.1130/G34929.1>
- Vera, J. A., & Coord (2004). Cordillera Bética y Baleares. In J. A. Vera (Ed.), *Geología de España* (p. 884, Map. 1). Madrid: Sociedad Geológica de España & Instituto Geológico y Minero de España.
- Verga, D., & Premoli Silva, I. (2002). Early Cretaceous planktonic foraminifera from the Tethys: The genus *Leupoldina*. *Cretaceous Research*, *23*, 189–212. <https://doi.org/10.1006/cre.2002.0309>
- Verga, D., & Premoli Silva, I. (2003a). Early Cretaceous planktonic foraminifera from the Tethys: The small, few-chambered representatives of the genus *Globigerinelloides*. *Cretaceous Research*, *24*, 305–334. [https://doi.org/10.1016/S0195-6671\(03\)00045-4](https://doi.org/10.1016/S0195-6671(03)00045-4)
- Verga, D., & Premoli Silva, I. (2003b). Early Cretaceous planktonic foraminifera from the Tethys: The large, many-chambered representatives of the genus *Globigerinelloides*. *Cretaceous Research*, *24*, 661–690. <https://doi.org/10.1016/j.cretres.2003.07.007>
- Verga, D., & Premoli Silva, I. (2005). Early Cretaceous planktonic foraminifera from the Tethys: The upper Aptian, planispiral morphotypes with elongate chambers. *Cretaceous Research*, *26*, 239–259. <https://doi.org/10.1016/j.cretres.2005.01.004>
- Vergès, J., & García-Senz, J. (2001). Mesozoic evolution and Cainozoic inversion of the Pyrenean Rift. In P. A. Ziegler, W. Cavazza, A. H. F. Robertson, & J. Crasquin-Soleau (Eds.), *Peri-tethys Memoir 6: Peri-Tethyan Rift/Wrench basins and Passive margins. Memoirs 186*. Paris, France: Muséum National d'Historie Naturelle.
- Wagner, T., Wallmann, K., Herrle, J., Hofmann, P., & Stuesser, I. (2007). Consequences of moderate ~25,000 yr lasting emission of light CO<sub>2</sub> into the mid-Cretaceous ocean. *Earth and Planetary Science Letters*, *259*, 200–211. <https://doi.org/10.1016/j.epsl.2007.04.045>
- Weissert, H. (1989). C-isotope stratigraphy, a monitor of paleoenvironmental change: A case study from the early Cretaceous. *Surveys in Geophysics*, *10*, 1–61.
- Weissert, H. (2000). Deciphering methane's fingerprint. *Nature*, *406*, 356–357. <https://doi.org/10.1038/35019230>
- Weissert, H. (2019). Mesozoic C-cycle perturbations and climate: Evidence for increased resilience of the Cretaceous biosphere to greenhouse pulses. *Canadian Journal of Earth Sciences*, *56*, 1366–1374.
- Weissert, H., & Erba, E. (2004). Volcanism, CO<sub>2</sub> and palaeoclimate: A Late Jurassic–Early Cretaceous carbon and oxygen isotope record. *Journal of the Geological Society*, *161*, 695–702. <https://doi.org/10.1144/0016-764903-087>
- Weissert, H., Joachimski, M., & Sarnthein, M. (2008). Chemostratigraphy. *Newsletters on Stratigraphy*, *42*, 145–179. <https://doi.org/10.1127/0078-0421/2008/0042-0145>
- Weissert, H., Lini, A., Föllmi, K. B., & Kuhn, O. (1998). Correlation of Early Cretaceous carbon isotope stratigraphy and platform drowning events: A possible link? *Palaeoogeography, Palaeoclimatology, Palaeoecology*, *137*, 189–203. [https://doi.org/10.1016/S0031-0182\(97\)00109-0](https://doi.org/10.1016/S0031-0182(97)00109-0)
- Weissert, H. J., & Lini, A. (1991). Ice age interludes during the time of Cretaceous Greenhouse climate? In D. W. Muller, J. A. McKenzie, & H. J. Weissert (Eds.), *Controversies in modern geology* (pp. 173–191). London: Academic Press.
- Westermann, S., Stein, M., Matera, V., Fiet, N., Fleitmann, D., Adatte, T., & Föllmi, K. B. (2013). Rapid changes in the redox conditions of the western Tethys Ocean during the early Aptian Oceanic Anoxic Event. *Geochimica et Cosmochimica Acta*, *121*, 467–486.
- Wezel, F. C. (1985). Facies anossiche de episodi geotettonici globali. *Giornale di Geologia*, *47*, 281–286.
- Wissler, L., Funk, H., & Weissert, H. (2003). Response of Early Cretaceous carbonate platforms to changes in atmospheric carbon dioxide levels. *Palaeoogeography, Palaeoclimatology, Palaeoecology*, *200*, 187–205. [https://doi.org/10.1016/S0031-0182\(03\)00450-4](https://doi.org/10.1016/S0031-0182(03)00450-4)
- Wissler, L., Weissert, H., Buonocunto, F. P., Ferreri, V., & D'Argenio, B. (2004). Calibration of the Early Cretaceous time scale: A combined chemostratigraphic and cyclostratigraphic approach to the Barremian–Aptian interval, Campania Apennines and Southern Alps (Italy). In B. D'Argenio, A. G. Fischer, I. Premoli Silva, & H. Weissert (Eds.), *Cyclostratigraphy: Approaches and case histories* (Vol. 81, pp. 123–133). Tulsa, OK: SEPM Special Publication Society for Sedimentary Geology.
- Wissler, L., Weissert, H., Masse, J.-P., & Bulot, L. (2002). Chemostratigraphic correlation of Barremian and lower Aptian ammonite zones and magnetic reversals. *International Journal of Earth Sciences*, *91*, 272–279. <https://doi.org/10.1007/s005310100210>